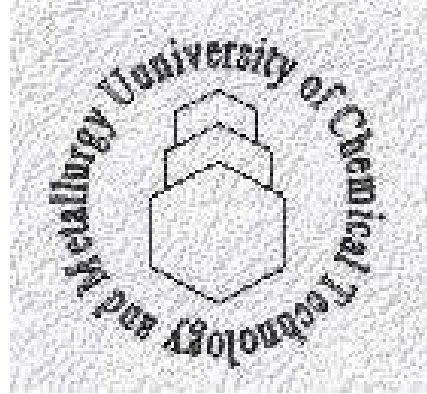


**Escuela Técnica
Superior de Ingenieros
Industriales de Vigo**



**University of Chemical
Technology and
Metallurgy**



Master thesis

**ELECTRODEPOSITION OF CERIUM
CONVERSION COATINGS FOR
CORROSION PROTECTION OF AA2024
ALLOY**

Erasmus Student

José Aníbal Piñeiro Ayuso

Acknowledgements

I would like to express my gratitude to Assoc. Prof. Dr. M. Machkova, Prof. DSc. Dr. Vl. Kozhukharov for been always available to help me and specially to Assoc. Prof. Dr. I. Nenov and Dr. S. Kozhukharov for been working hand by hand every day, and because without them this work would not be possible.

Also, I want to convey thanks to the EC– ERASMUS office and from the Bulgarian NSF, contract DVU-02/102, particularly to Gustavo Pelaez for the chance to live this enriching experience.

I.	LITERATURE REVIEW	5
1.	Industrial classifications and standards of the aluminium alloys	5
2.	Uses and properties of AA2024	6
3.	Economic impact caused by the corrosion phenomena	7
4.	Corrosion processes, Basic concepts	7
5.	Structural features of AA2024 T3 aluminium alloy	12
6.	Coating systems, composition and classifications	13
7.	Correlations among the features of the Cerium conversion coatings and conditions of deposition	16
	i. Adhesion to the substrate	17
	ii. Thickness of the coating	18
	iii. Density of the coating	18
	iv. Structure and composition of the coatings	19
8.	Mechanism of the corrosion processes on the aluminium alloys	22
9.	Electrochemical characterization of coated systems	27
II.	AIM AND TASKS OF THE WORK	34
III.	EXPERIMENTAL	35
1.	Composition of the metallic substrates	35
2.	Preliminary treatment of the metallic substrates	35
3.	Conditions of Cerium conversion coatings depositions	36
	i. Composition of the Cerium conversion coatings bath	36
	ii. Regime of Cerium conversion coatings deposition	37
4.	Measurements and characterizations	37
	i. Equipment for electrochemical research activities	37
	ii. Equipment for non-electrochemical characterization	40
	iii. Conditions of electrochemical measurements	41
IV.	RESULTS AND DISCUSSION	42

1. Impact of the preliminary treatment on the quality of the Cerium conversion coatings deposition	42
2. Conditions of Cerium conversion coatings depositions	47
i. Influence of the concentration of the basic substance of the conversion bath on the features of the Cerium conversion coatings	47
ii. Influence of oxidant addition, and deposition current on the features of the Cerium conversion coatings	49
iii. Superficial morphology observations	58
V. CONCLUSIONS	67
VI. REFERENCES	68

I. LITERATURE REVIEW

1. Industrial classifications and standards of the aluminium alloys

Generally, all of the industrial products should correspond to some conventions, describing the requirements, for the properties of given industrial product. These conventions, known also as “Standards”, ensure the utility of the respective products. By that manner, each standard serves as guarantee for the safety and reliability of the respective products and the materials, composing them. Nowadays, due to the globalization of the markets, the conventional standards become international, Aluminium 2024-T351; AA2024-T351,; UNS A92024 (according to United Numbering system) ; ISO AlCu4Mg1 (regarding the International Organisation of Standardisation) [1]; [2]; AA2024-T4, ASME SB211; as ISO – for European Community; GOST 172342 - 99 [3]for Russian federation; CSA CG42 (Canada), NF A-U4G1 (France); DIN AlCuMg2 (Germany); LY12 for China [4], etc.

Usually, each standard is composed by the Code name of the respective product (or material), recommendation or brief description for the methods applied for its production, and brief description of the basic properties, which should possess the respective product (material).

According to [5] the aluminium alloys are named “AA”, with four digit numbers, revealing their compositions, and permitted levels of contamination. Additional numbering could sign the method applied for metallurgical post-treatment.

Table 1. Nomenclature of the aluminium alloy according to [5]

Code of the Aluminium alloy (AA)	Concentration of the main alloying element
AA1XXX	99.0% minimum;
AA2XXX	Copper (1.9%...6.8%);
AA3XXX	Manganese (0.3%...1.5%);
AA4XXX	Silicon (3.6%...13.5%)
AA5XXX	Magnesium (0.5%...5.5%);
AA6XXX	Magnesium and Silicon (Mg 0.4%...1.5%, Si 0.2%...1.7%);
AA7XXX	Zinc (1%...8.2%);
AA8XXX	Others

2. Uses and properties of AA2024

AA2024T351 is commonly used in the manufacture of truck wheels, aircraft structures, and screw machine products, scientific instruments, veterinary, orthopedic braces and equipment, and in rivets. That is because it has good machining characteristics and a fair cold formability which make it one of the best options for cold heading and thread rolling applications as we can see in tables 2 and 3. [6,7]

Table 2. Typical mechanical properties [6]

Temper	Tensile (.500" Dia. Specimen)					Hardness Brinell 500 kg 10 mm	Shear		Fatigue*		Modulus	
	Ultimate		Yield		Elongation/4D %		Ultimate Shearing Strength		Endurance Limit - R.R. Moore Type		Modulus of Elasticity	
	KSI	MPa	KSI	MPa			KSI	MPa	KSI	MPa	KSI x 10 ³	Gpa
0	27	186	11	76	22	47	18	124	13	90	10.6	73.1
T4, T351	68	469	47	324	19	120	41	283	20	138	10.6	73.1
T6	69	476	57	393	10	125	41	283	18	124	10.6	73.1
T851	70	482	65	448	7	128	43	296	18	124	10.6	73.1

Table 3. Comparative characteristics [7]

Temper	Corrosion Resistance		Cold Workability ³	Machinability ³	Anodize Response ³	Brazeability ⁴	Weldability ⁴		
	General ¹	Stress ²					Gas	Arc	Spot
T4, T351	D	C	C	B	C	D	C	B	B
T6	D	B	C	B	C	D	D	C	B
T851	D	B	D	B	C	D	D	C	B

1 Ratings A through E are relative ratings in decreasing order of merit, based on exposures to sodium chloride solution by intermittent spraying or immersion. Alloys with A and B ratings can be used in industrial and seacoast atmospheres without protection. Alloys with C, D and E ratings generally should be protected at least on faying surfaces

2 Stress-corrosion cracking ratings are based on service experience and on laboratory tests of specimens exposed to the 3.5% sodium chloride alternate immersion test.

A= No known instance of failure in service or in laboratory tests.

B= No known instance of failure in service; limited failures in laboratory tests of short transverse specimens.

C= Service failures with sustained tension stress acting in short transverse direction relative to grain structure; limited failures in laboratory tests of long transverse specimens.

D= Limited service failures with sustained longitudinal or long transverse areas.

3 Ratings A through D for Workability (cold), A through E for Machinability and A through C for Anodize Response, are relative ratings in decreasing order of merit.

4 Ratings A through D for Weldability and Brazeability are relative ratings defined as follows:

A= Generally weldable by all commercial procedures and methods. B= Weldable with special techniques or for specific applications that justify preliminary trials or testing to develop welding procedure and weld performance. C= Limited weldability because of crack sensitivity or loss in resistance to corrosion and mechanical properties. D= No commonly used welding methods have been developed.

3. Economic impact caused by the corrosion phenomena

The effects of corrosion are present in our lives, directly affecting the useful service lives of our possessions, and indirectly incurring in corrosion costs for producers and suppliers of goods and services, which affect final consumers. Some consequences are economic, and cause the following: [8]

- Replacement of corroded equipment
- Overdesign to allow for corrosion
- Preventive maintenance, for example, painting
- Shutdown of equipment due to corrosion failure
- Contamination of a product
- Loss of efficiency
- Loss of valuable product
- Inability to use otherwise desirable materials □
- Damage of equipment adjacent to that in which corrosion failure occurs

4. Corrosion processes, Basic concepts

Corrosion refers to a process that involves deterioration and subsequent degradation of the metals [9]. Most corrosion phenomena are of electrochemical nature and consist of at least two reactions on the surface of the corroding metal. One of the reactions is the oxidation, referred as the anodic partial reaction, and the other is a reduction reaction, referred as the cathodic partial reaction.

All the electrochemical process possesses generally heterogeneous character. This fact means that the superficial area of the interface between the solid material (i.e: The metal or metallic alloy), and its environmental medium (which could be liquid, gaseous or even aerosols).

That is the reason for the great importance of the state of the interface, predetermined by its superficial morphology (roughness), and its chemical

composition. The surface chemical composition depends on the chemical elements represented there, their quantities and their distribution.

Each of the features described above of the metallic surface are consequence of different stages of metallurgic production: (i)-The chemical composition of the metal depends on the fusion, (ii) The structure of the metal is predetermined by the metallurgic post treatment procedures (Forging, molding, etc.), (iii) -The roughness depends on other post treatment procedures, like cold rolling, hot rolling, etc. Finally, each stage of the metallurgic production predetermines all the features of the produced alloys, such as: The composition (during the fusion), the structure (thermal post treatment), the roughness (hot and cold rolling).

Matter and Co. [10] have developed a brief study regarding the influence of the superficial preliminary treatments and even chemical modifications on the behavior of AA2024 plates in a model corrosive medium. For their purpose, they have compared three groups (five plates in each). The first group was only degreased, the second one has passed subsequent mechanical treatment after the degreasing, and at last the third one underwent degreasing, mechanical and final chemical treatment.

As a result, they have established that the metal plates have obtained different superficial topographies and even chemical compositions, as is shown in Figure 1:

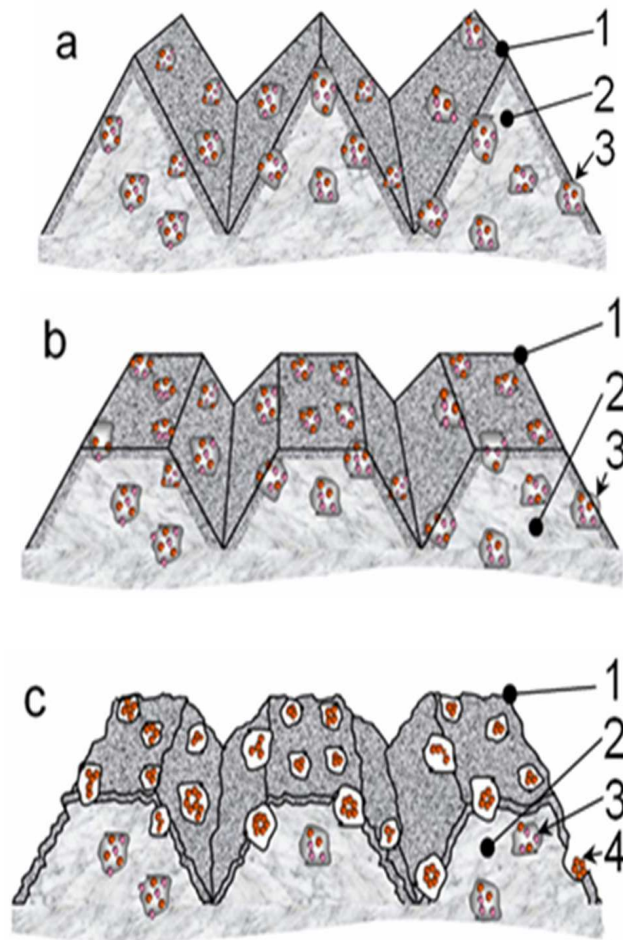


Figure. 1. Schematic views of superficial morphologies of the samples; a – as received; b – after polishing; c – after polishing and etching [10]

1 – Native oxide layer; 2 – basic aluminium matrix; 3 – Al₂CuMg S-phase intermetallic precipitates; 4 – Copper remnants from the S-phases, after the chemical treatment.

As could be seen from this visual model in fig. 1, the mechanical treatment (i.e: polishing), results in decrease of superficial roughness, whereas the chemical treatment involves supplemental chemical modification. As a result, the latter approach of preliminary treatment causes distinguishable compositions on the surface and in the bulk of the material.

Both the roughness and the superficial possess tremendous influence on the behavior of the alloy in corrosive medium. Thus, the differences of the superficial morphologies have been confirmed by Atomic Force Microscopy observations, shown in figure 2:

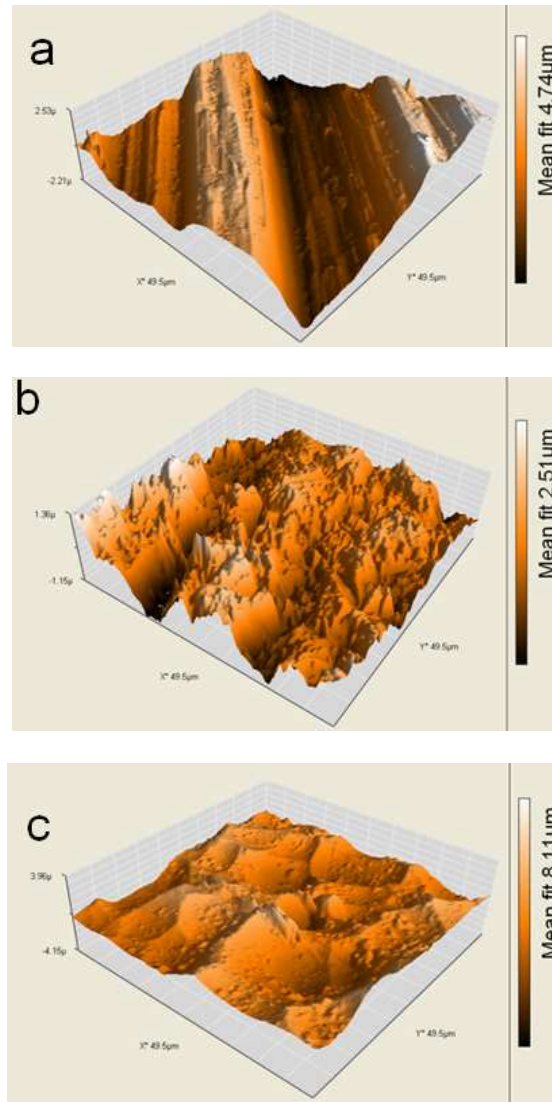


Figure. 2. Superficial morphologies of the samples; a – as received; b – after polishing; c – after polishing and etching [10]

Indeed, apparently different morphologies have been obtained by the authors after the respective preliminary treatment procedures. The untreated surface possesses laminar shape, obtained during the rolling in the producer. After the mechanical polishing the morphology has suffered remarkable conversion, and large number of small pyramidal features appeared. The last one reveals wide zones occupied by craters. They are result of the aggressive chemical attack by the NaOH solution, during the chemical etching.

Furthermore, the authors have concluded that these surfaces have significant influence on the rate and even the mechanisms of the corrosion processes.

The authors have also established that the superficial treatments have a strong influence on the structure and the thickness of the native oxide layer. Usually, in the metallurgical industries, the metals suffer thermal post-treatments, in order to achieve more equal distribution of the internal mechanical tensions. This treatment should have impact on the surface oxide layer, as well. The oxide layer is described to be composed by various Al – O compounds, as for example: Al_2O_3 , $\text{Al}(\text{OH})_3$, and/or $\text{AlO}(\text{OH})$ [11], [12], [13]. Additionally, the oxide layer is rather multilayered system, composed by thin corundum underlayer, and porous upper layer, as is described elsewhere [14]. There, the authors mention the application of the Al-oxide layer for humidity sensors, because of its aptitude for water uptake, as consequence of presence of highly developed porosity.

Other authors [15] have performed research on the various chemical preliminary treatments in alkaline or acidic solutions, before deposition of cerium conversion coating via spray deposition. As main result, the authors conclude that surface preparation prior to spray deposition had a significant effect on the thickness of the subsequent cerium based conversion coating.

Additionally, they have concluded that the protective capabilities of once applied cerium conversion coating, deposited on preliminary acid-activated AA2024 excels even 40 layered coating on alkaline activated one.

The control of the thickness and structure of the Alumina superficial layer could be controlled by electrochemical methods, as well, as is described elsewhere [16].

5. Structural features of AA2024 T3 aluminum alloy

According to the standards, this alloy should have a nominal composition, as is described above. During the metallurgical processes, all the alloying elements form intermetallic precipitates, due to the limited solubility of the respective elements in the aluminum matrix. According to Rao and co. [17] the intermetallic inclusions are classified into: coarse particles, and fine precipitates. Besides, they mention that both kinds of precipitates are formed in different stages of the metallurgical production. The former are formed during the initial solidification of the metallurgical fusion, whereas the latter are rather consequence of the post metallurgical treatments (i.e: aging processes).

The basic feature which enables to distinguish their compositions. The majority of them belong to the so called “S-phase”, composed by Al_2CuMg . This intermetallic’s precipitate covers almost 3% of the geometrical surface area of AA2024 alloy, The second type of intermetallics which occurs in the alloy’s composition is $Al_{16}(Cu, Fe, Mn)$ constituting 12% of all the precipitates. Minor concentrations of $Al_{20}Mn_3Cu_2$, $Al_{12}Cu$, $Al_{17}Cu_2Fe$, and $(Al, Cu)_6Mn$ are present in the alloy as well. Besides them there are other intermetallics, such as: θ – phase, composed by Al_2Cu . All kinds of intermetallics except S-phase are composed of metals nobler than aluminium, thus showing cathodic character. However, the S-phase is composed of nobler copper as well as of active magnesium [18]. In the literature is mentioned that, all the aluminum alloys in which their grain size decreases, involves a decrement in the corrosion rate [19-23].

Also, other studies determined that UFG (ultra-fine-grained) Al alloys which contain second phases or precipitates exhibit a decrease in the number of observed pits with ECAP(equal-channel angular pressing) processing due to either a decrease in the size, or fragmentation of precipitates[19, 24-27].

6. Coating systems, composition and classifications

The coating systems could be divided in various groups, according to their chemical compositions, and/or deposition methods.

According to the former classification basis, they could be divided into, organic, modified organic, hybrid and completely inorganic, as is described by K. Heinz and H. Rose [28].

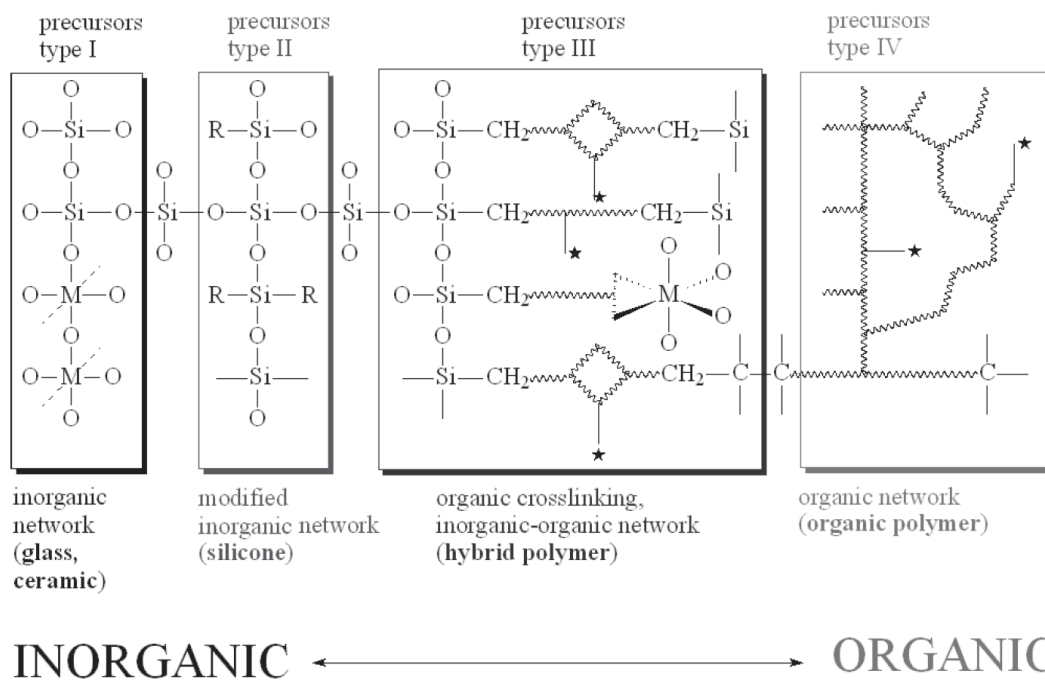


Figure 3. Classification of the materials, according to their compositions [28]

Usually, the natures of the substrate and the coating material respectively predetermine the most appropriated approach for deposition of the coating. Principally, the methods could be also divided into Spray assisted methods, electrochemical methods, high temperature methods, etc.

Furthermore, the coating systems could be mono, or multilayer, where the latter enable combination of properties of different layers, composing the coating system.

In the aircraft industry, it is commonly accepted to apply multilayered, multifunctional coatings, as is shown in the figure below.

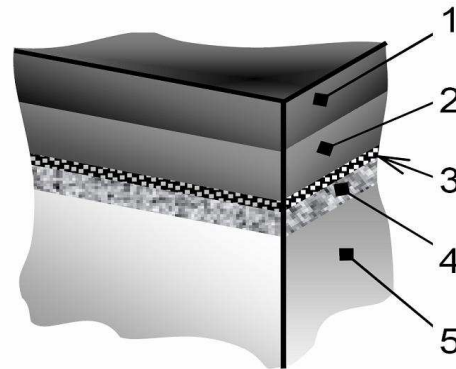


Figure. 4. Schematic presentation of multilayer coating system according [29].

1,2 – finishing double layer of polyurethane, 3 – intermediate adhesive layer; 4 – primer hybrid coating; 5 – metal substrate

Another important characteristic of the coatings is the “self-healing” ability. This property should provide protection effects even after partial disruption of the coating. This ability could be achieved by addition of active substances that could precipitate after reaction with corrosive species, or corrosion products. This class of substances is known as “corrosion inhibitors”. In that means, Cr(VI) compounds, mainly chromates, are widely applied as corrosion inhibitors for a wide range of metals and alloys, such as aluminium alloys [30 – 35]. During decades, the chromate conversion coatings have been used as primer layers. Their efficiency-cost ratio has made them standard corrosion inhibitors, during several decades [36].

However, it is established that the chromate compounds are highly toxic and carcinogenic [37, 38]. This fact has led to severe restrictions regarding the usage of chromium compounds in different countries. Particularly, in European Community, the employment of chromium compounds is forbidden in the

automobile industry by “*End life vehicles*” (EVL) directive since 2004 [39]. Furthermore, this prohibition is preceded by the “*Restriction of Hazardous Substances*”, edited at 2002 year, for the electric and electronic industry [40]. These directives are in correspondence to the general politics undertaken by United Nations regarding the environmental protection (UNEP), followed by directives as (*Integrated Pollution Prevention and Control - IPPC*) and *CEPE* [41, 42].

These directives have stimulated world-wide scientific research activities for environmentally friendly alternatives of the chromium compounds in the corrosion protective coatings. In that means, the lanthanides have proven to be rather efficient inhibitors [43], and also their level of toxicity is not recognized to be considerable [44, 45]. Another reason for the great interest regarding the Ce-compounds is the fact that these substances are considered to be economically compatible [46], predetermining the reasonability of their application in the industrial practice. The inhibition efficiency of various salts of the rare-earth cerium in form of trivalent ions, such as cerium nitrate ($\text{Ce}(\text{NO}_3)_3$) [47 – 50], cerium chloride (CeCl_3) [51 - 57], cerium sulphate ($\text{Ce}_2(\text{SO}_4)_3$) [58, 59], and others [60 – 68].

7. Correlations among the features of the CeCC coatings and the conditions of their deposition

Undoubtedly, there is direct relation among the characteristics, the method, and the conditions of production of whatever industrial product, as is mentioned elsewhere [69, 70]. This conjunction predetermine the behaviour of

the corresponding product, and on the other hand, they depend strongly on the features of the equipment used. This conjunction is represented on figure 5:

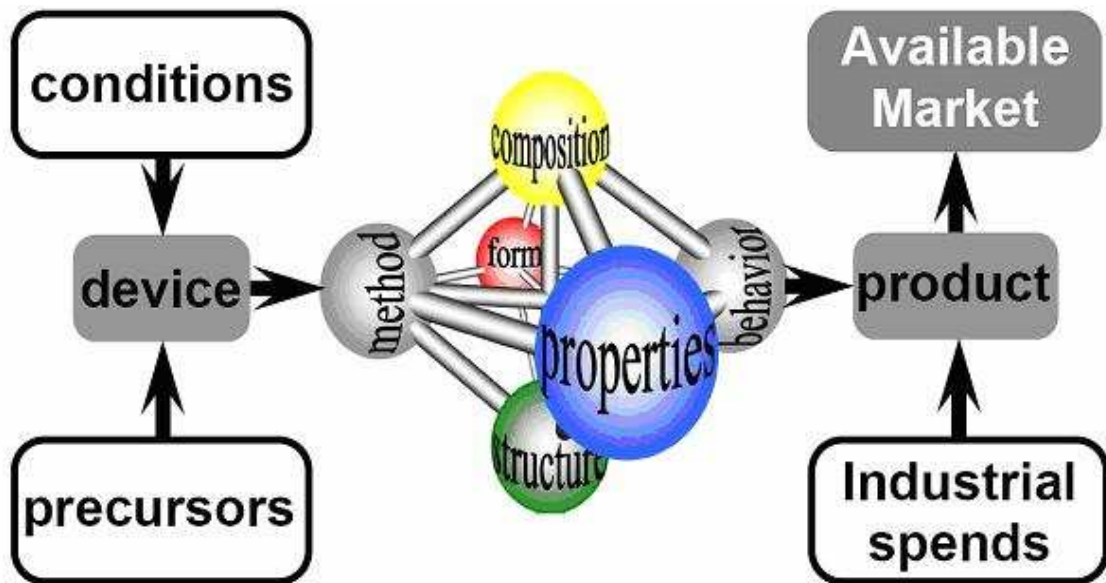


Figure. 5. Conjunction among the features, behaviour and conditions of production

In the case of CeCC, their behavior could be described by the combination between the corrosion protective ability and durability [71]. In turn, they depend on the properties of the respective coating, such as thickness, density and adhesion to the metallic substrate. Another factor of great importance is the distribution of the thickness; the coating undoubtedly should possess a form of continuous film on the metallic surface, instead of island like, which is observed very often in the CeCC coatings. The coatings should also possess crack free structures with equal distribution of the metallic oxides and hydroxides in their compositions. At last, several methods could be applied for coating deposition: spin coating, dip coating, brush painting and electro deposition.

i. Adhesion to the substrate: This property depends generally on the state of the metallic surface, prior to deposition of the coating. Consequently, the most important factors that influence on the coating adhesion are: the chemical

composition of the metal substrate, and the structure of the superficial oxide layer. Another important feature of the metallic substrate is the roughness and the superficial morphology. The larger number of edges and peaks should provide better adsorption ability of the metallic surface.

Indeed, Hinton [72] mentions that the deposition relies on electrochemical interactions between the aluminum matrix and intermetallic inclusions that make up structural aluminum alloys. Here should be mentioned that the superficial composition could be modified by aggressive (alkaline or acidic) solutions. Generally, in the literature it is preferred to apply the sequence of degreasing, desmutting and acidic activation (degusing) [73, 74].

This sequence is preferred by the majority of the researchers, although in some cases only mechanical treatment has been applied prior to film-deposition [75, 76]. Furthermore, various receipts for chemical preliminary treatments are available in the literature [77 – 79]. Usually, the preliminary treatments could be performed by commercial chemicals, as is described elsewhere [80]. However, the quality of the preliminary treatments depends on the compositions of the solutions used, as well as on the conditions of the treatment (i.e: temperature and duration of exposure of the specimens). For that reason, Rivera and co. [81] have compared different durations and temperatures of exposition to commercial solutions. Finally, it should be mentioned that the procedures of preliminary treatment and the respective effects on the subsequent deposition are object of special investigations [82]. The authors have reached the conclusion that only once deposited film after acidic activation, excels forty-layered coating, after alkaline etching.

Geng and co. [83] represent entire scheme of the diverse approaches for preliminary treatment, as is shown on the figure below:

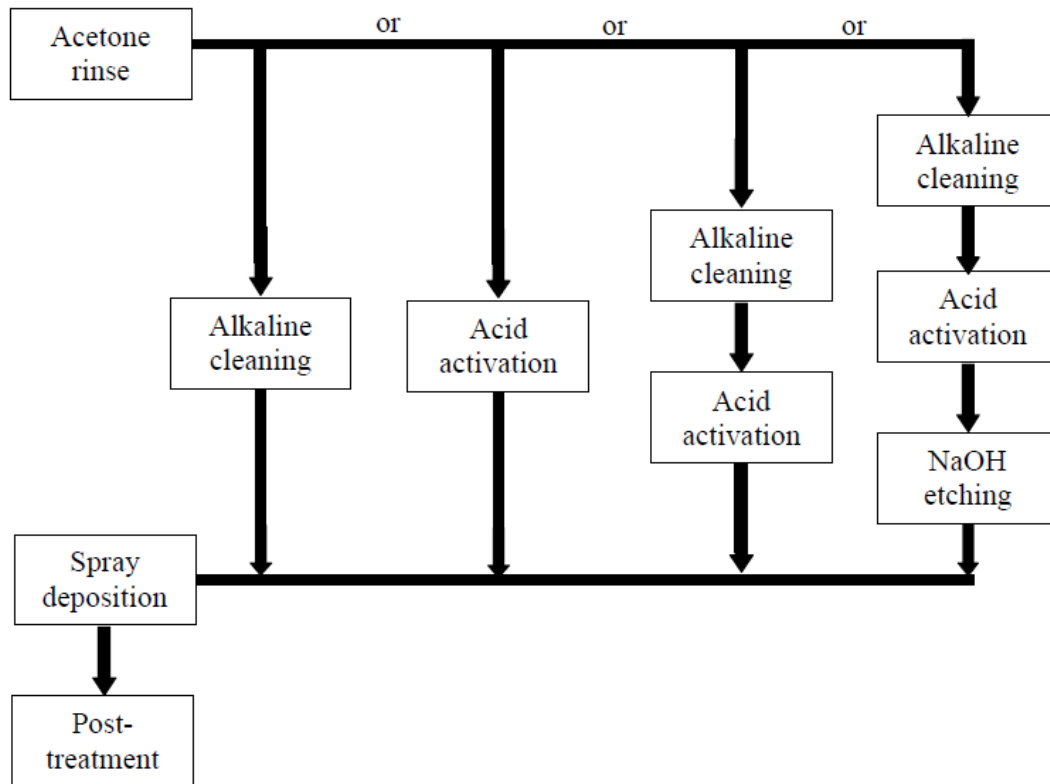
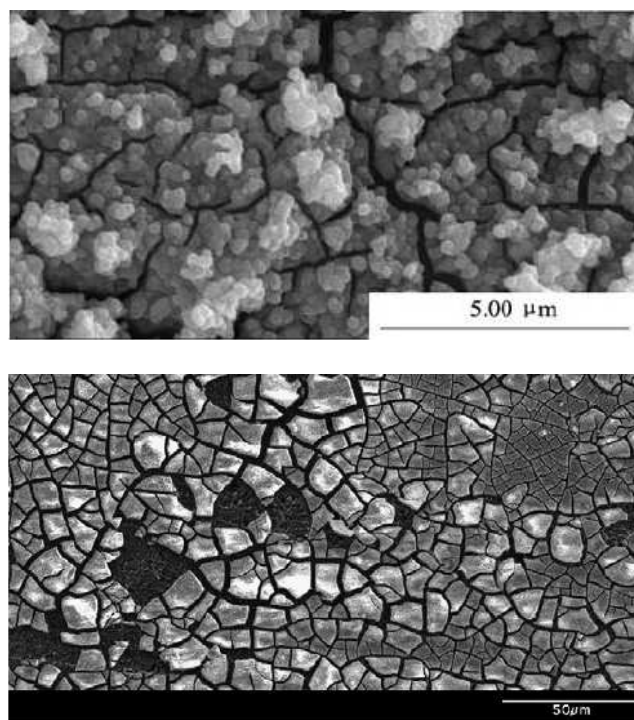


Figure. 6. Schematic presentation of the various approaches of superficial treatment prior coating deposition [83]

ii. Thickness of the coating: Usually, the extended number of depositions, and/or enlarged deposition time should contribute to higher thickness. However, in the particular case of electrodeposition of cerium conversion coatings there is a limit, related to the fact that after one moment a dense layer of Ce-oxides/hydroxides forms. Afterwards, it represents a barrier for deposition of further charged particles (i.e: Ce-ions) towards the metallic matrix.

iii. Density of the coatings: This group of coatings should not vary in large range of densities, because these coatings are mainly composed by cerium oxides/hydroxides. Nevertheless, it depends on the structure of the aluminum oxide, which is predetermined by preliminary treatments, as is discussed above. Additionally, if the currents applied during the deposition are too high then colloidal precipitates could be attracted, besides charged particles. This phenomenon could lead to obtaining of friable porous coatings.

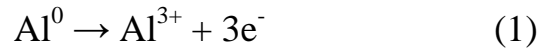
iv. Structure and composition of the coatings: As was mentioned above in the present work, the structure and composition of the coatings is directly related to the method, and the conditions, applied for deposition. On the other hand, they predetermine the properties, and consequently – the behavior of the obtained films. On the next figure, micrographs obtained by Scanning Electronic Microscopy of two CeCC coatings are represented



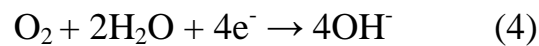
**Figure. 7. SEM images of CeCC, obtained by different methods
a – electrodeposition [75]; b – spray deposition [82]**

Ordinary, the CeCC have cracked structure, but in the good barrier-formed coatings, the cracks are not enough deep to reach the metallic surface. Furthermore, the cracked structures favor the adhesion of the next layers in the coating system.

The CeCC coatings are generally composed by cerium oxides and hydroxides, originated from the conversion of the respective water-soluble cerium salts, according to the following reactions [80]:

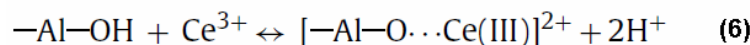
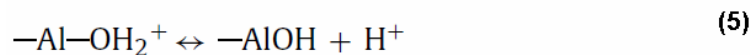


The dissolved oxygen in the solution also could participate in reactions, being reduced - producing additional quantities of hydroxyl ions [84]:



All of these reactions lead to formation of insoluble products of Cerium oxides/and hydroxides. Here should be mentioned that according to the conditions, these products could form either precipitates (undesirable product), or layer deposition (the aimed product).

Consequently, Conde and etc. [85] remark that the obtaining of desirable covering layer passes through chemisorption processes on the superficial oxide layer of the aluminum that could be described in brief, as follows:



According to them, this chemisorption process passes via formation of intermediated complexes on the metallic surface, such as: $\text{Al}-\text{O}-\text{Ce}-(\text{OH})_2^{2+}$. This supplemental process is crucial for the formation of adherent protective film instead of colloidal precipitates and sediments in the solution.

Taking into account that the superficial oxide layer of the aluminium consists simultaneously of: Al_2O_3 , $\text{Al}(\text{OH})_3$ and $\text{AlO}(\text{OH})$ phases [75], it could be accepted that the composition of the oxide layer has extreme importance for the formation of well defined adherent protective layer, instead of precipitates and sediments. The oxide layer as structure and composition depends so on the preliminary treatment applied, so on the pH of the medium during the deposition. That is the reason to accept that the pH of the deposition solution is

the key factor for obtaining of adherent protective films of CeCC. The structure of the oxide layer is irregular, and composed of sub-layers of various aluminum oxides and hydroxides, as is depicted in the next figure:

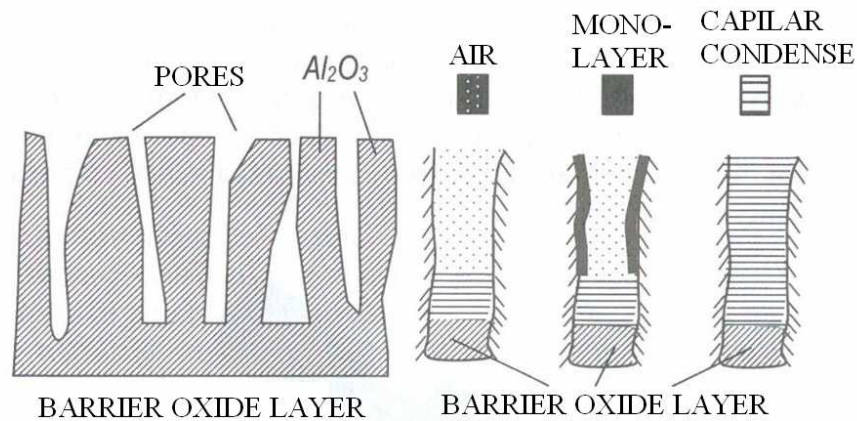


Figure. 8. Schematic presentation of Al-oxide layer [13]

At last, the cerium conversion coatings could be modified by addition of supplemental substances, for densification of their structures. These supplements could be either introduced directly to the coating solution [82], or in post treatment procedure [86]. In the former case, the authors have added gelatin to the main Ce-solution, whereas in the latter case, additional phosphating procedure has been applied, in order to achieve further stabilization of the already obtained coating.

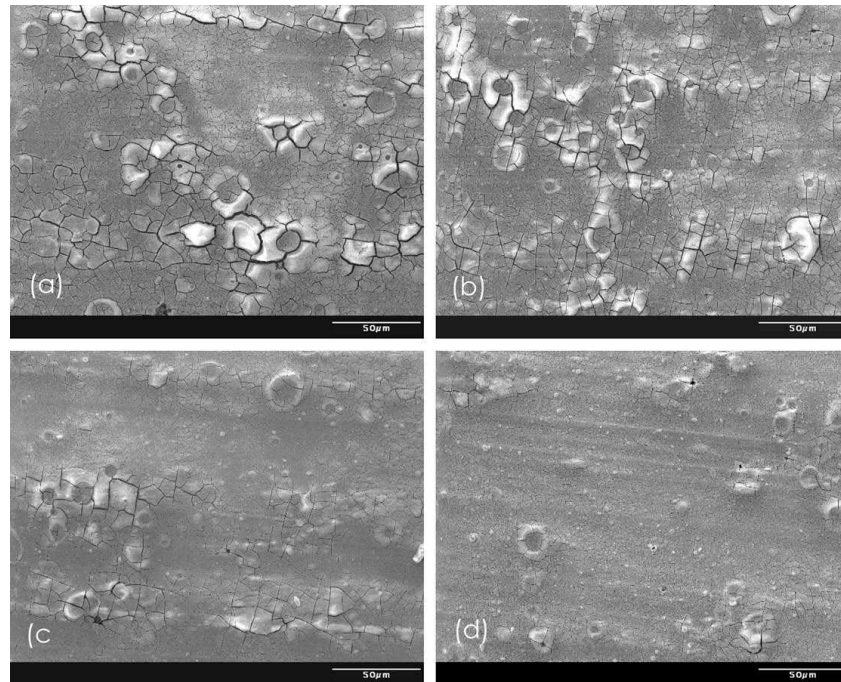


Figure. 9. SEM micrographs of CeCC, post-treated for 5 min at different temperatures (a) - as-deposited, (b) - 55 °C, (c) - 70 °C, (d) - 85 °C [86].

As could be seen from the figure, the coatings possess much more dense and crack-free structures, after appropriated post-treatments (positions c and d). Nevertheless, the additional supplements could enter in undesirable reactions with the main ingredients of the deposition solutions, provoking decrement of their stability, and the additional procedures lead to increase of time and financial expenses.

8. Mechanism of the corrosion processes on the aluminum alloys

In chloride containing environment, the most active metals (Al and Mg) represented in the superficial S-phase intermetallic particles (Al_2CuMg), which were found on the alloy surface, suffer selective or chemical dissolution [18] (Eqs. 7 and 8), as it is shown in Figure. 10.

This process leads to changes in both of the solid S-phase, and the liquid medium (in that case solution of NaCl). The medium becomes more alkaline, while the S-phase loses Al, and Mg components and consequently, copper-enriched particles are formed and start to behave as micro-cathodes.

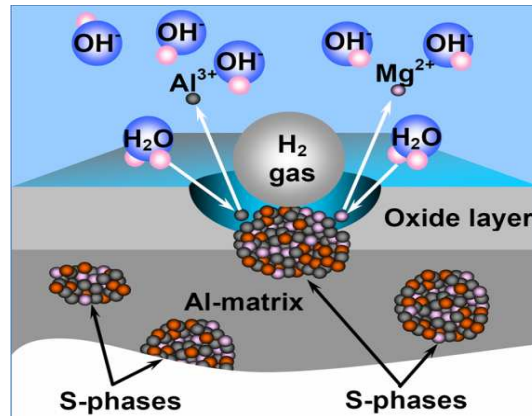
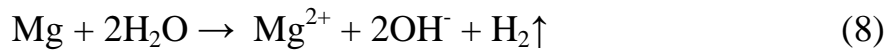
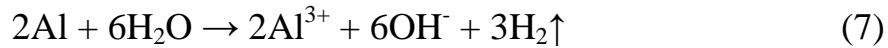


Figure. 10 Selective dissolution of Mg and Al from S-phase intermetallics

These changes convert the process from purely chemical to electrochemical (i.e: the second stage begins) according to Yasakau [18].



The second stage is dominated by electrochemical process, which recognized by another author [87] to be the first stage of the pitting corrosion of AA2024, where clear cathodic and anodic areas are formed. Then, the reactions on the respective areas are, cathodic oxygen reduction reaction on copper-rich remnants and anodic oxidation or dissolution reaction of the both more active metallic elements aluminium (Eq. 7) and magnesium (Eq. 9).



Simultaneously, the aluminium cations Al^{3+} , product of reaction (7), react with the hydroxyl anions OH^- from the liquid medium, forming sediments of $\text{Al}(\text{OH})_3$ by passing through intermediate product $\text{Al}(\text{OH})_4^-$, as is shown on the figure below:

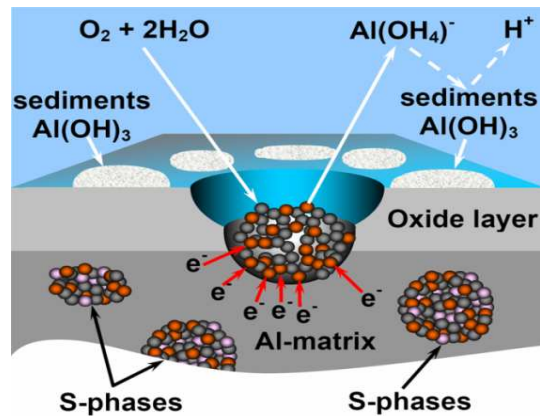
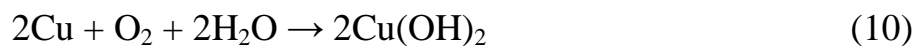


Figure. 11. Second (electrochemical) stage of corrosion of S-phase

Continuous dissolution of aluminium and magnesium leads to deeper dealloying of the S-phase and form very porous structure “Swiss cheese”-like morphology with copper particles connected to the copper remnants [50].

Consequently, the processes accelerate continuously, and the third stage begins. When the neck between a copper nanosized particle and a remnant is broken, the particle loses the electrical contact with the alloy. Then the chemical reaction of copper oxidation by dissolved oxygen is thermodynamically possible:



Partial dissolution of the copper hydroxide occurs due to formation of hydroxo complexes. The complex ions then are electrochemically reduced again to metallic copper when contact with the surface of the aluminium alloy or with the copper remnants formed after dealloying as is shown in Fig. 12. The formation of chloride-based complexes can also assist the dissolution of copper particles. The reduced metallic copper redeposited on the copper remnants leads to copper “refining” [50]. When copper redeposited on the alloy surface around pits, it forms a thin cathodic film.

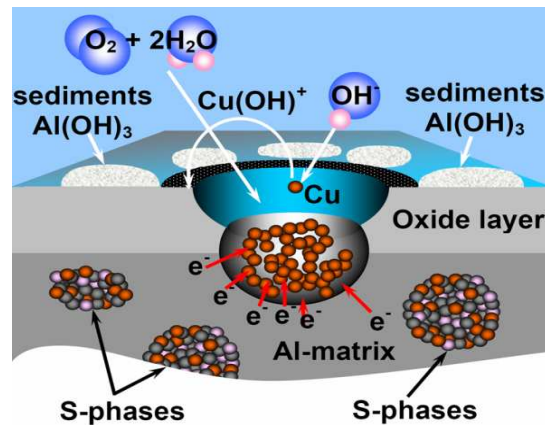


Figure. 12. Third stage of corrosion of S-phase intermetallic particles

Another mechanism for this process was proposed ascribing migration of Cu particles from dealloyed intermetallic over the pit [88]. The thin layer of copper redeposited around pits could play a role of an additional cathode accelerating the anodic processes of aluminium dissolution from the S-phase and from the surrounding alloy matrix (Fig. 13), which is depleted in copper and thus is anodically active. The localized corrosion process becomes thus autocatalytic. Therefore, re-deposition of copper appears as a very important factor responsible for fast propagation of pits around intermetallics, consequently leads to formation of corrosion ulcer (Fig. 13).

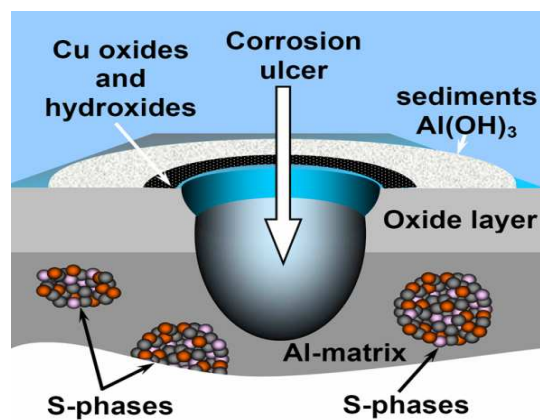


Figure. 13. Formation of the corrosion ulcer

Other authors have divided corrosion observed on the surface into two types of attack sites, including localised corrosion which involved isolated particles [89] and co-operative corrosion [90]. The co-operative corrosion events were characterised by domes of corrosion product within a ring of corrosion product. The central domes appeared to be anodically active sites, since chloride was often observed there as well as H₂ evolution, and at least some of them were initiated by the coupling between S-phase and cathodic intermetallic particles within the surface.

It should be mentioned that the chemical and electrochemical corrosion processes on the AA2024 alloy's surface possess much more sophisticated mechanism, predetermined by the simultaneous presence of various intermetallic precipitates, as is described in [89]. The highest concentration among these intermetallics belongs to the S-phase. Hughes et al. [90] report that they have found simultaneous presence of nine different intermetallic precipitates with clearly distinguishable compositions, based upon (Al, Cu)_x(Fe, Mn)_ySi. All of these inclusions are potential initiators of local corrosion, due to the simultaneous presence of nobler and more active metals, which form cathodic and anodic areas, respectively.

In summary, it is clear that the S-phase intermetallics not only function execution as a cathode or as an anode in the corrosion processes but also play a complex role combining cathodic and anodic activity together in the same particle.

9. Electrochemical characterization of coated systems

Basic point in the technical sciences is the characterization of various parameters and their quantification via measurements. In that means, each scientific investigation is based on comparison of different key-features of the investigated products and their elucidation in accordance with change of parameters and conditions of their synthesis and preparation.

By the other hand, in the industrial practice, each new product must undergo detailed characterization, in order to describe its behaviour in the condition of its exploitation. This includes so the initial its characteristics so their changes within the time of its usage. Generally, all characterizations are related to whatever kind of measurements.

The measurement could be considered as a quantitative comparison of given parameter with given reference from the same nature [91].

Practically, the measurements could be performed directly or indirect manner. The latter one consists on measurement of another parameter, which stays in direct functional dependence with the parameter which values should be determined.

In electrochemistry, the references used are generally *referent electrodes*. Here should be mentioned that the most basic referent electrode is the hydrogen electrode. Its construction is given in Figure 14.

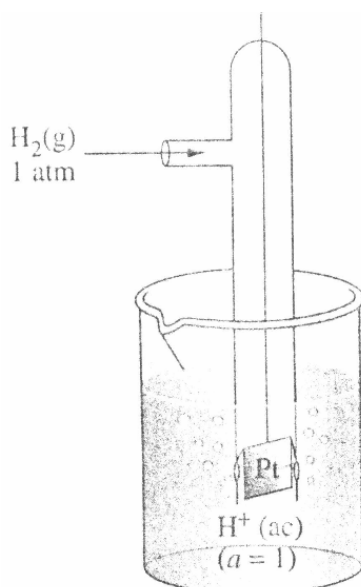


Figure. 14 Basic construction of hydrogen referent electrode [91]

Because of the considerable difficulties, related to its maintenance, other referent electrodes have been entered in the practice. Figure 15 represents various commercially available electrodes.

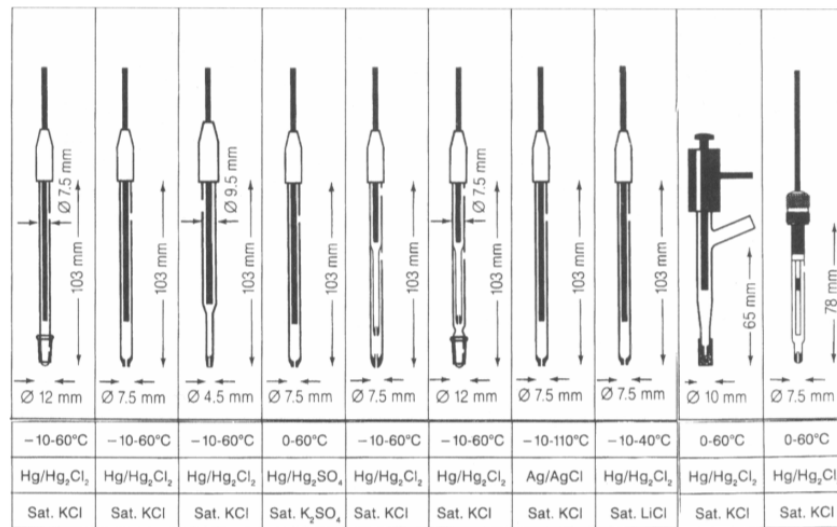


Figure. 15. Examples for various commercial referent electrodes [93].

Thus, with the technological progress, the measuring systems have been also developing continuously. This development has enabled to enlarge the number and variety of electrochemical parameters, which could describe the processes occurring in given electrochemical system.

The simplest measuring system could be composed by only an electrochemical cell, connected with Voltmeter. It enables measurement of the potential of the respective electrode, compared with this of a referent electrode, as is shown in Fig.16 (a). If the performance of the measurement is requires application of external source of electromotive power, or current, then additional counter electrode is necessary. It is connected to electric chains which involves input signals from the automatic device to the respective cell (fig. 16 (b)).

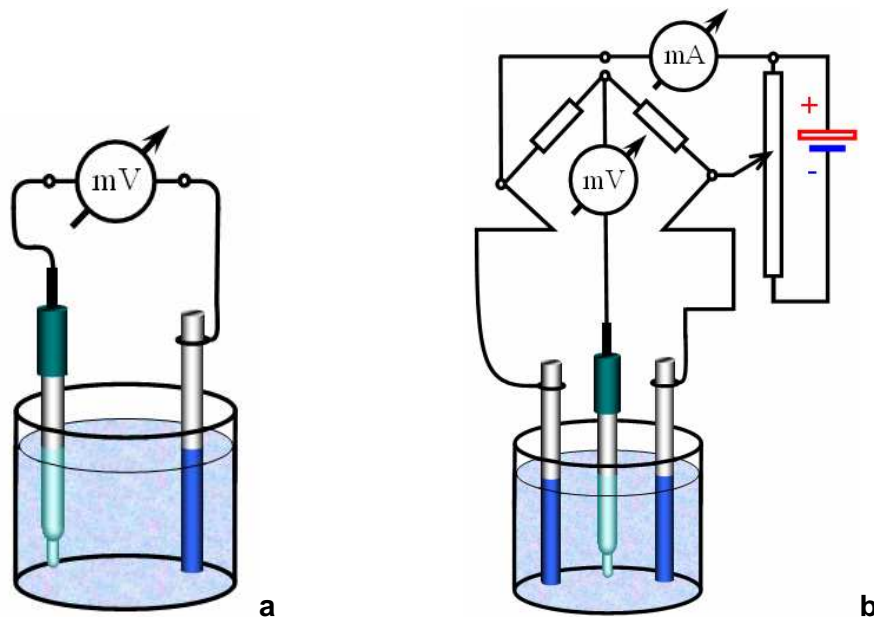


Figure. 16. Electrical circuits for electrochemical measurements

a – simple system; b – system with counter electrode

The employment of a counter electrode enables to execute various regimes of electrochemical measurements. In brief, they could be classified into the following groups:

Potentiostatic: When the current to- or from- the sample (serving as working electrode), is measured according to the reference electrode for given potential value, determined by the device.

Galvanostatic: When the potential to- or from- the sample (serving as working electrode), is measured according to the reference electrode for given current, determined by the device.

When the measurements include predetermined gradual variation of the respective input parameters, these regimes are known as “potentiodynamic” and “Galvanidynamic”.

Practically, all electrochemical measurements, and processes require use of electrochemical cells. Additionally, there are requirements for the cells as

well. They must provide equal distribution of electric fields to each point of the respective electrodes. The counter electrodes always must be composed by noble metals (like Pt, Au, Ag), in order to avoid undesirable contamination of the electrolyte by whatever corrosion products from the counter electrode.

Different schemes for the most classical two electrode (Fig. 17 (a), and 17 (b)) and three electrode (Fig. 18 (a), and 18 (b)) cells are represented below.

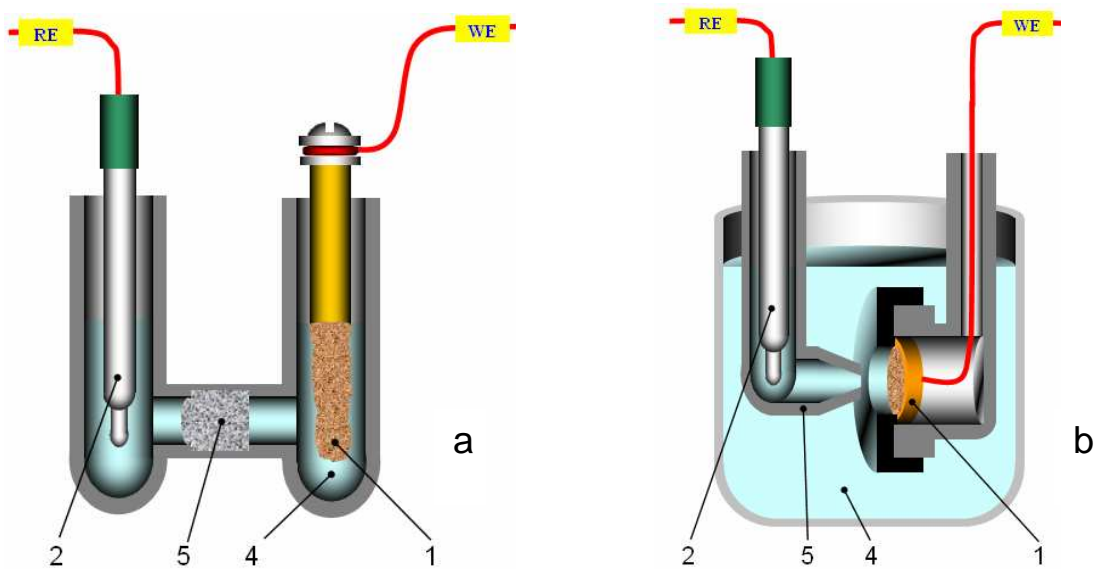


Figure 17. Schematic presentations of two electrode cells a – for cylindrical working electrode; b – for disk-shaped working electrode

1 – Working electrode; 2 – refence electrode; 4 – electrolyte; 5 – filter or Luggine capillary

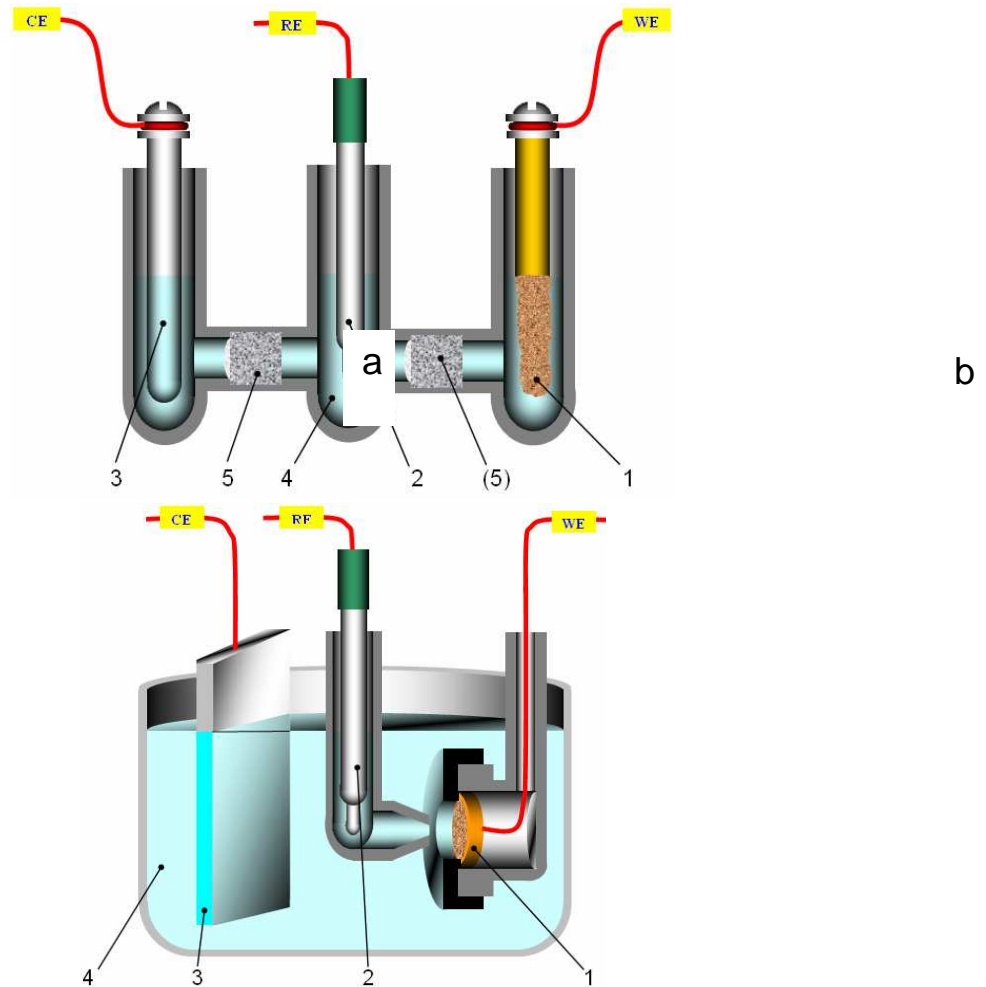


Fig. 18. Schematic presentations of three electrode cells

a – for cylindrical working electrode; b – for disk-shaped working electrode

1 – Working electrode; 2 – reference electrode; 3 – counter electrode; 4 – electrolyte; 5 – filter or Lugin capillary

The systems with three electrode cells enable determination of the polarization resistance by introduction of linear (gradual) variation of the respective signals.

-Optical microscopy: The optical microscope, often referred to as the "light microscope", is a type of



conventional optical

microscope which uses visible light and a system of lenses to magnify images of small samples. Optical microscopes are the oldest design of microscope and were possibly designed in their present compound form in the 17th century by Antonie van Leeuwenhoek [92]. The microscopes could have various constructions, but they could be divided into two groups:

-Microscopes with transmitted light: In their case, the observed image is a result of the light transmitted through the observed object. This kind of microscopes is used in microbiology. Figure 19 shows photography of such kind of microscope.

-Microscopes with reflected light: In their case, the observed image is a result of reflected light from the observed sample. This kind of microscopes is used generally in metallography.

-Scanning Electronic Microscopy: The SEM is a developed as successor of the Transmission Electronic Microscopy (TEM). Both of these kinds of microscopy are based on the interaction of an accelerated electron beam and the surface of the observed sample. As result, three kinds of derivative signals appear: (i) – Back Scattered Electrones – these are the electrons from the initial beam that are reflected from the surface of the sample. (ii) – Secondary electrons – The origin from the atomic electron shells of the compositional elements of the sample, which are expelled by the initial beam. (iii) – Characteristic X-ray waves. They are also produced by the lose of kinetic energy of the electrons from the initial beam, after its collision with the particles composing the specimen. The analysis of this kind of derivative radiation stays in the basis of the Energy Dispersive X-ray spectroscopy. Additional thermal and visible radiations also appear as consequence of the interactions of the initial beam with the sample.

The next figure shows schematic presentation of a classical TEM device.

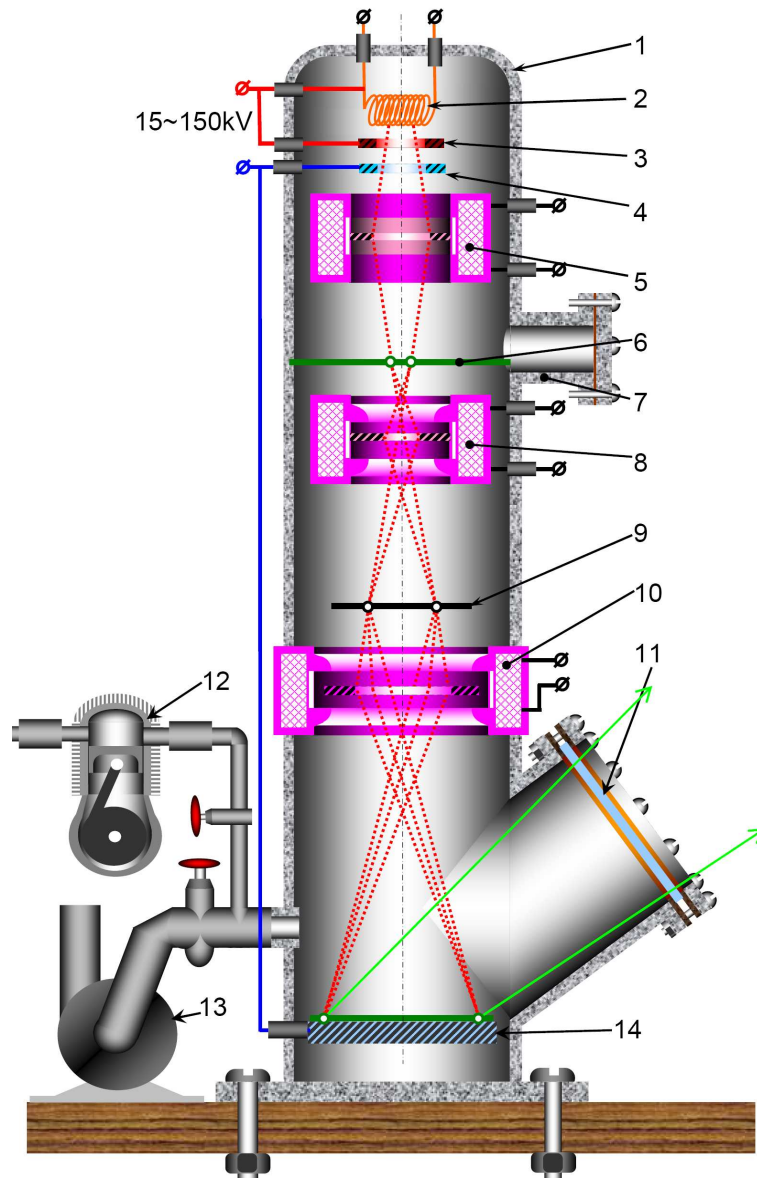


Fig. 20. schematic presentation of a classical TEM device

1 – Corpus; 2 – source of the initial beam (cathode); 3 – electrode for fixing of the contrast; 4 – accelerating electrode; 5 – beam driving coil; 6 – sample holder; 7 – port for the sample; 8 – beam driving coil;

9 – initial image; 10 – second beam driving coil; 11 – window for observation with thick lead containing glass; 12, 13 – vacuum pumps; 14 – Target with coverage of ZnS (anode).

II. AIM AND TASKS OF THE WORK

The aim of the present research work is to investigate a new cerium compound, for cathodic electrodeposition of Cerium based conversion coatings (CeCC) for protection of AA2024 alloy against corrosion. The cerium salt - Diammonium pentanitrocerate $((\text{NH}_4)_2\text{Ce}(\text{NO}_3)_5)$ was used, where the Cerium is represented in the anionic moiety, instead of all the rest electrolytes used up to nowadays.

For achievement of the basic purpose of the present work, the following tasks were undertaken:

1. Determination of the influence of the preliminary treatment on the AA2024 specimens on the properties of the CeCC coatings.
2. Determination of the optimal concentration of $((\text{NH}_4)_2\text{Ce}(\text{NO}_3)_5)$ in the electrodeposition solution.
3. Optimization of the H_2O_2 content in electrolyte for electrodeposition.
4. Optimization of the electrodeposition regime:
 - a. Density of the currents applied for electrodeposition
 - b. Continuation of the electrodeposition process.
5. To characterize the superficial morphology and composition of the CeCC by Optical Metallographic Microscopy (OMM) and Scanning Electronic Microscopy (SEM) combined with Energy Dispersive X-ray spectroscopy (EDX).

6. To assess the barrier ability and durability against corrosion of the coatings by electrochemical methods – Linear Sweep Voltammetry (LSV), and Electrochemical Impedance Spectroscopy (EIS).

III. EXPERIMENTAL

1. Composition of the metallic substrates

All substrates were composed of aluminium aircraft alloy, D 16AM, described in GOST 172342 – 99. According to [95], this alloy is typical presenter of the AA2024, produced in Ukraine, and delivered by: Kloeckner Metalsnab AD, (Bulgaria) web Page : http://www.metalsnab.com/en/news/iso_cert.php

Because the standards allow some deviations from the basic nominal composition, the Al-sheet has passed an additional analysis, in order to determine the exact composition. The composition of the alloy was determined by Inductively Coupled Plasma Optical Emission Spectroscopy (ICP-OES) using a standard procedure and presents in Table 4.

Table 4. Composition of AA2024 alloy according to ICP – OES analysis.

Element	Al	Cu	Fe	Mg	Mn	Ni	Si
Concentration (wt.%)	Residual	3.716	0.404	1.259	0.537	0.055	< 0.01

In Central Laboratory of Scientific Research “Geohimia”, to Ivan Rilsky UNIVERSITY OF MINING AND GEOLOGY "ST. IVAN RILSKI"; <http://www.mgu.bg/main.php?menu=2&submenu=18&labs=7>.

All the samples for the present research work were cut in form of squares with linear size 60 mm, and 3mm of thickness.

2. Preliminary treatment of the metallic substrates

Various combinations of conditions were applied for deposition of CeCC. In that manner, the coating on each sample possessed, unique individual combination of conditions.

The conditions of CeCC deposition could be divided in various combinations, as follows: mechanical, mechanical and alkaline etching, and mechanical and acidic activation.

- Mechanical preliminary treatment: The samples D16 AM samples were submitted to wet-polish, by SiC emery papers with 240, 500, 800, 1000, 1200 grits, subsequently. Afterwards, they passed washing by tap, and distilled water. Finally, they were degreased by immersion in pure acetone for 10 minutes at room temperature, and final vigorous cleaning by tap water for at least 1 minute followed by distilled water.

- Alkaline preliminary treatment: After polishing up to 1000 grits emery paper, the samples underwent etching by immersion in NaOH solution (50 g/l) at 55 °C for 5 minutes. The last stage of the procedure was performed by immersion in diluted HNO₃ (1:1) for 5 minutes, at ambient temperature. Before each stage of the procedure, the samples passed cleaning by vigorous tap-water, followed by distilled water.

-Acidic treatment procedure: Initially the samples were polished by emery papers until 1000. This procedure was followed by degreasing in acetone, according the conditions described above (in the previous procedures). Afterwards, the samples were acidically etched by 260 g/l H₂SO₄ solution (i.e: 133ml of 95% sulfuric acid are dissolved in up to 1 liter by distilled water), for 5 minutes at 50 °C, following the emergency rules. Finally, the samples were cleaned by tap water, and distilled water, as is described in previous procedure.

3. Conditions of CeCC depositions

i. Composition of the CeCC bath

The basic composition of the conversion bath was aqueous solution of diammonium pentanitrocerate - (NH₄)₂Ce(NO₃)₅ and oxidant H₂O₂. In this Ce-

compound the cerium ion is included in the anionic compositional part, in difference of all nowadays described in the literature Ce-species, where the Cerium is in form of simple Ce-salts – basically CeCl_3 . The basic compound was selected to be in three different molar concentrations: 0.01; 0.05; and 0.1 mol/l of $(\text{NH}_4)_2\text{Ce}(\text{NO}_3)_5$ in distilled water. The quantity of the oxidant (30% H_2O_2) varied in the following concentrations (ml/l): 10, 20, 25, 50 and 100. For this range of the basic solution and the oxidant, the pH varied in the range from 2.36 to 3.7.

ii. Regime of CeCC deposition

The electrodepositions were performed at cathodic currents in Galvanic static regime with the following current densities (mA/cm^2): -1, -2, -3, and -5, and at 3, 5, and 7 minutes of duration. All of the depositions were executed at ambient temperature.

4. Measurements and characterizations

i. Equipment for electrochemical research activities

The electrodepositions, together with the characterization of the deposited films were performed by potentiostat/galvanostat PG-stat “AUTOLAB” 30, supported by frequency response analyser “FRA 2”, produced by “Ecochemie” – (the Netherlands).

The pH values of the solutions, used for deposition were measured by HI 255 combined meter, produced by Hanna Instruments (USA), for determination of pH values, a universal glass electrode, produced by the same firm.

Electrochemical cells: Different cells were used for deposition and characterization: The former was the original flat cell of the Autolab, whereas for the latter case, three-electrode flat cells developed in LAMAR - laboratory were employed. Both of them are represented in Fig. 21.

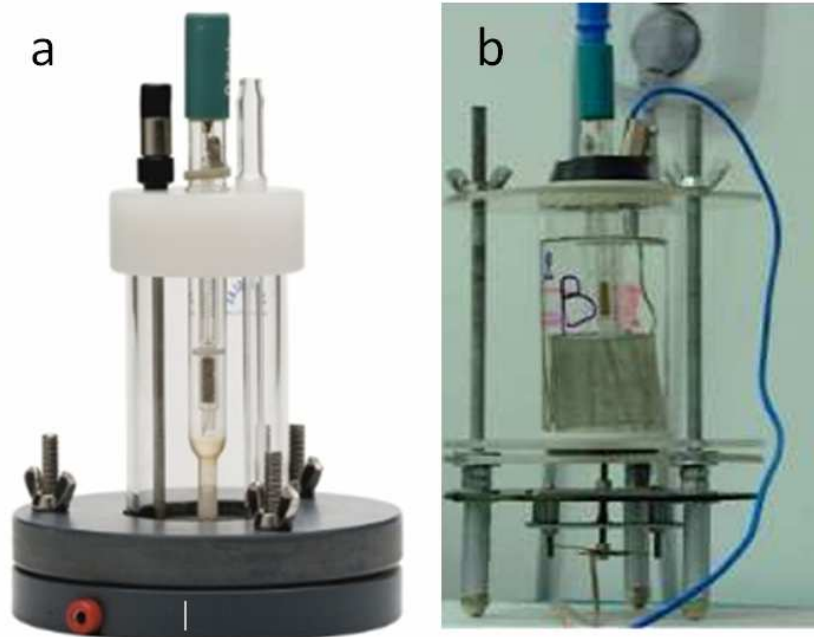


**Fig.21. Photographies of the electrochemical cells used
a-cell used for electrodeposition; b – cell used for measurements**

The cells were in three electrode configurations, where each electrode has its proper function, as follows:

Reference electrode: For reference electrodes were used Ag/AgCl -3M KCl, commercial electrodes, model 6.0733.100, product of Metrohm (Netherlands).

Counter-electrodes: A cylinder-shaped platinum net with highly developed superficial area was used for counter electrode in the measurement cells. The “horseshoe” – shaped counter electrode, was used for the needs of electro-deposition. This shape enabled parallel surface to the sample, for achievement equal distribution of the thickness of the coating layer.

Working electrodes: Limited zones from the alloy samples served as working electrodes. For electro-deposition, the exposed to the coating solution area was with 12 cm². After the deposition, the samples with the deposited films were mounted in the measurements cells. In this case only 2 cm² of the deposited film was exposed to the model corrosive medium. It was composed by 3.5_{wt.} % of NaCl in distilled water.

This difference between the exposed areas in the respective cases for the deposition and measurements is consequence of two reasons: (i) – the lower diameter in the second case allows to avoid whatever edge-effects, related to the coating; (ii) – the larger difference between the surface areas of the working electrodic zone and this of the counter electrode permitted to avoid influence of the CE-capacitance during the Electrochemical Impedance Spectroscopy; (iii) the smaller area in the case of the measurements permitted to select more than one zone of the coating.

In order to avoid whatever “edge” – effect, the working zones in the deposition (fig. 21 (a)), and measuring (fig. 21 (b)) were with different diameters, as is shown in Fig 22.

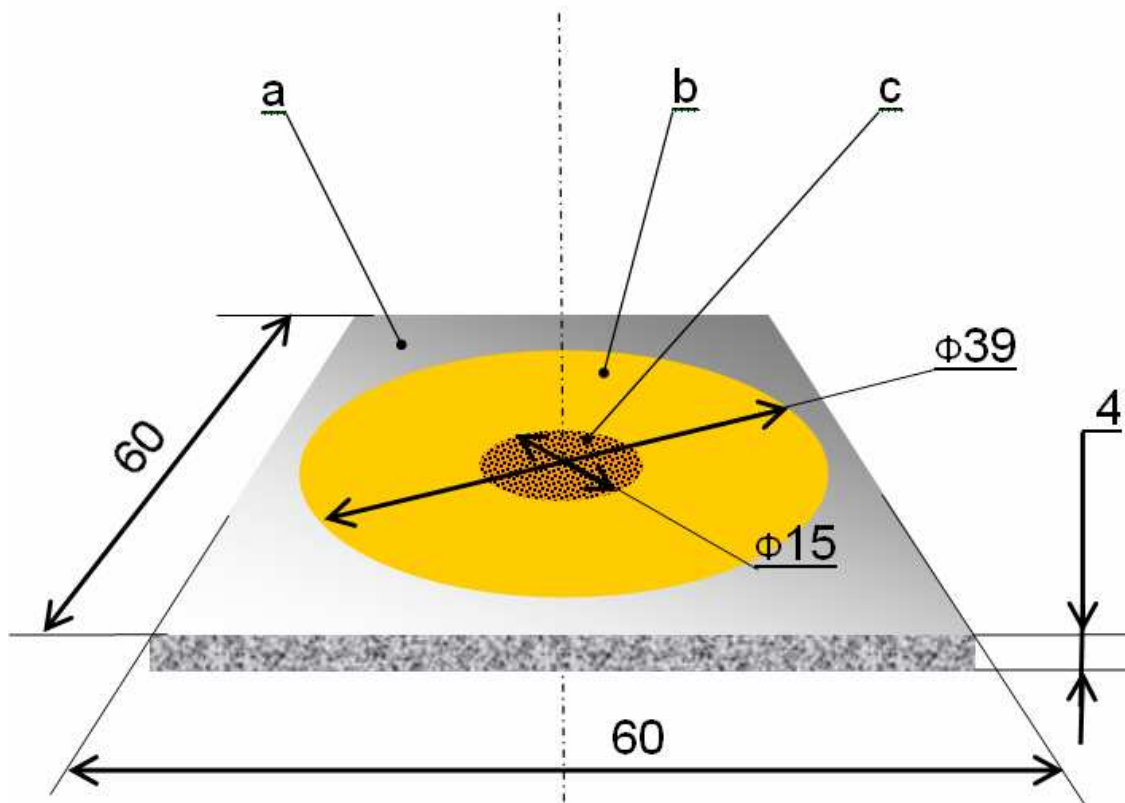


Figure. 22. Schematic view of the samples after the depositions and measurements
a – AA2024 metallic substrate; b – electrodeposited CeCC coating; c – Zone of corrosion tests

ii. Equipment for non-electrochemical characterization

For completeness of the research activities, the samples were characterized via Optical and Scanning Electronic Microscopy.

Optical Microscopy: It was performed by Microscope “BoeCo”- (Germany), at low (100x) and high (400x) rates of magnification. The microscope was directly connected by a web-camera, in order to obtain images.

Scanning Electronic Microscopy: The observations via SEM were executed only on the best samples (i.e.: these specimens, that showed the highest barrier abilities and durabilities). The superficial morphologies of the separate samples before and after immersion in the solutions with and without cerium inhibitors were observed at different magnifications using Scanning Electronic Microscopy (SEM), (TESCAN, SEM/FIB LYRA I XMU). The SEM observations were combined by Energy Dispersion X-Ray Spectroscopy (EDX), performed by E, (Quantax 200 of BRUKER detector), connected to the SEM-device. The equipment used for SEM-EDX observations and characterization is shown in fig.23.



Figure 23. Exterior view of a SEM-EDX device

iii. Conditions of electrochemical measurements

In order to minimize the working electrode polarization the electrochemical measurements were performed in the following subsequence: the initial polarization curves were acquired in a narrow interval around the Open Circuit Potential ($OCP \pm 0.03$ V), at a potential sweep range of 1mV/s. The values of R_p and E_{corr} were determined on the basis of these curves. Afterwards, the respective impedance spectra were acquired at the following conditions: frequency range from 10^4 to 10^{-2} Hz, distributed in 7 frequencies per decade, with signal amplitude of 10 mV according to OCP. At last, the individual cathodic and anodic polarization curves were recorded in a larger potential interval ($OCP \pm 500$ mV), at 1 mV/s potential sweep range. By maintenance of the sequence, no disgrace of the experimental data as a consequence of any electrode polarization could be admitted.

IV. RESULTS AND DISCUSSION

1. Impact of the preliminary treatment on the quality of the CeCC deposition

As is mentioned in the theoretical part of the present work, the preliminary treatment has crucial importance for the quality of the deposited film. This fact is consequence of the impact on both of roughness and superficial chemical composition of the substrates prior to the coating deposition. That is the reason to perform investigations on three samples with CeCC coatings deposited after: (a) - only mechanical polishing, (b) - mechanical + alkaline etching, and (c) - mechanical + acidic activation. Afterwards, the obtained samples (see Fig. 24) passed through measurements for determination of their barrier abilities and durabilities.



Fig. 24. Samples with CeCC films after different approaches of preliminary treatments, and posterior electrochemical measurements

After the respective procedures of preliminary treatment, the conversion coatings were electrodeposited at equal conditions of deposition (i.e.: 0.05 M $(\text{NH}_4)_2\text{Ce}(\text{NO}_3)_5$ with 30 ml/l of peroxide, 2 mA/cm², for 5 min.). In that manner, it was possible to perform comparative research on the impacts of the preliminary treatment procedures. These procedures are described in detail in section 2.1. of the experimental part of the present work.. The obtained samples were exposed to naturally aerated corrosive medium at room temperature, prior to execute the respective electrochemical measurements.

Figure 25 shows impedance spectra in Bode and Nyquist plots, recorded after 24 hours of exposition to 3.5% NaCl corrosive medium of three AA2024 samples

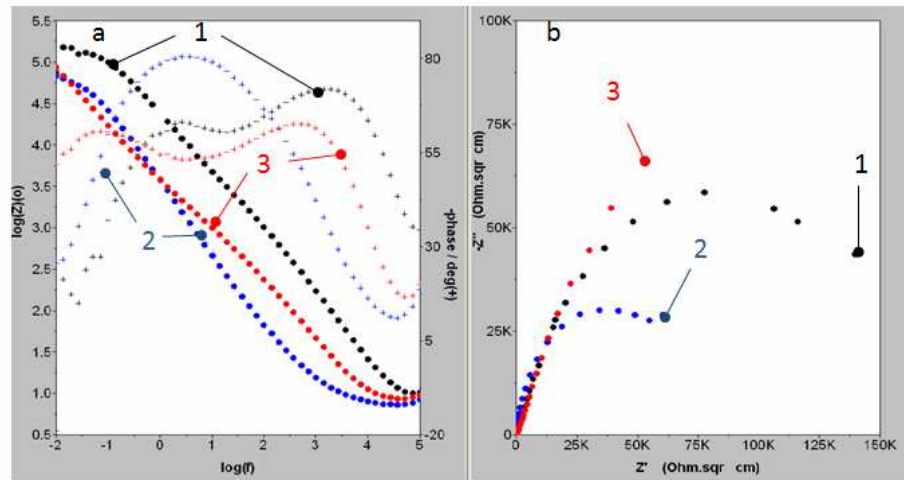


Fig. 25. Electrochemical Impedance spectra recorded after 24 hours of exposition of three samples with electrodeposited CeCC films after different approaches of preliminary treatment. a – Bode Plot; b – Nyquist plot 1-Alkaline; 2-Acidic; 3-Mechanical.

As can be seen from the figure, $\varphi = f(\log(f))$ curve of the sample after acidic pretreatment completely differs from the rest two. It possesses only one maximum that belongs to the native oxide film of the sample. The rest two $\varphi = f(f)$ curves (of the alkaline and mechanical preliminary treatments) have two clearly distinguishable maxima: of the oxide layer (in the range of 10^4 Hz) and of the electrodeposited films (between 1 and 10 Hz).

The $\log|Z| = f(\log(f))$ curve in the Bode plot, at 10^{-2} Hz of the sample with alkaline preliminary treatment is relatively higher than the rest two. In the Nyquist plot, the radius semi-circle of the sample with the alkaline treatment excels this of the sample with acidic pre-treatment. Both these facts indicate that the alkaline preliminary treatment leads to better barrier ability, compared to the mechanical and acidic approaches.

The results of the EIS spectra are confirmed by the linear sweep voltammetry. The anodic curve of the alkaline pre-treated specimen (see Figure 26) is situated at lower current densities, undoubtedly indicating that this approach leads to a better protection of the alloy after the subsequent coating.

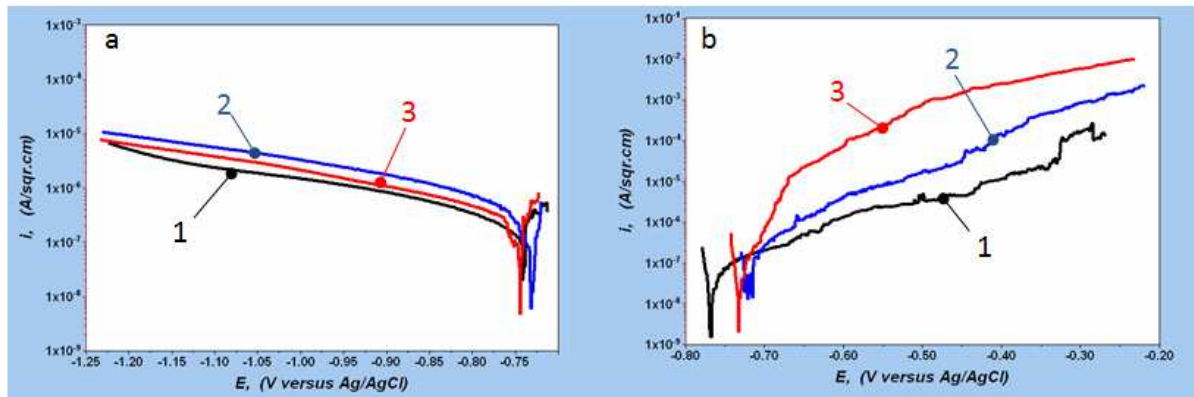


Figure. 26. Cathodic (a) Anodic (b) polarization curves recorded after 24 hours of exposition of three samples with electrodeposited CeCC films after different approaches of preliminary treatment. 1-Alkaline; 2-Acidic; 3-Mechanical.

Because the alkaline preliminary treatment predetermines the highest barrier ability of the coating, its durability was also tested. The evaluation of the durability was performed by exposition of the respective sample in naturally aerated 3.5% NaCl model corrosive medium at room temperature, and execution of electrochemical measurements once of week. The EIS spectra acquired during the exposition of the sample are represented in Fig. 27.

The semi-circles of the Nyquist plots decrease within the exposure time. Furthermore, their decrement is much more intensive during the initial 168 hours. The semi-circle recorded at the 24th hour has twice bigger radius than this, acquired at the 96th hour. The rest three semi-circles, recorded after 1, 2 and 3 weeks almost completely coincide, revealing that the corrosion process is hindered after 168 hours. The same trend is observable for the $\log|Z| = f(\log(f))$ curve in the Bode plot, at 10^{-2} Hz. The spectra acquired after the initial 24 and 96 hours, excel the rest, recorded after 1, 2 and 3 weeks, and the latter three curves overlap, as well.

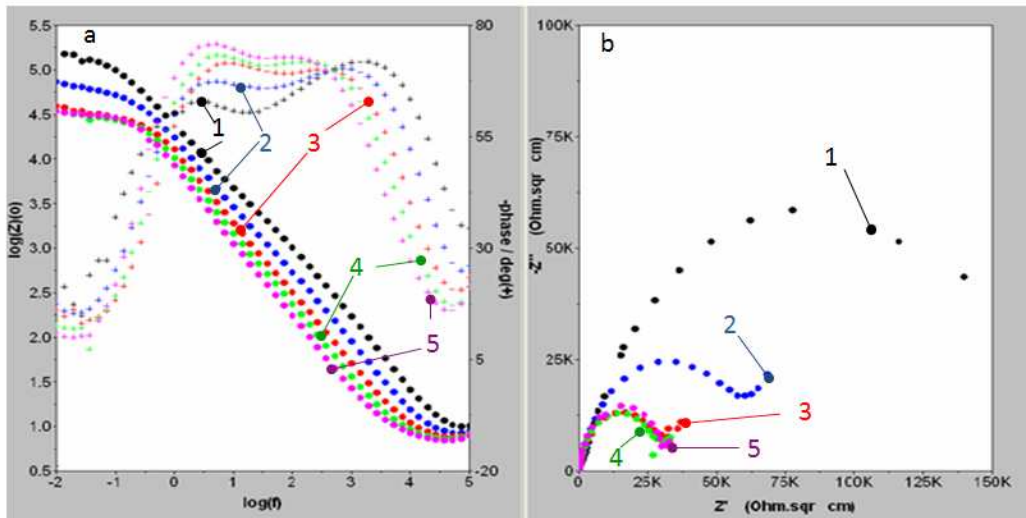


Fig. 27. Electrochemical Impedance spectra of AA2024 substrate after alkaline preliminary treatment recorded after different exposure times. a – Bode plot; b-Nyquist plot –. 1-24h; 2-96h; 3-168h; 4-336h; 5-504h.

The $\varphi = f(\log(f))$ curves in the Bode plots possess rather peculiar behavior. They are composed by two maxima, as was mentioned above. The maximum of the coating increases, within the exposure time, whereas this for the oxide layer remains almost unchanged. This fact is evidence for the increment of the capacitive resistance impact, because the phase shift approaches -90° . This phenomenon can be explained by densification of the coating. Because in the present case, the cerium is in form of insoluble layer, any inhibition effect could not be expected. So, it is much more probable to expect that the cracks of the coating are obstructed by corrosion products. They hinder the access of corrosive species to the metallic surface. As a result the coating improves its dielectric properties during the first 168 hours of exposure, and keeps them constant, at larger extensions of the exposition. Nevertheless, a small Warburg tails, revealing diffusion processes through the coatings.

The linear voltammograms of the sample coated after alkaline etching also show that the anodic curves, acquired for the almost entire exposition period overlap among themselves. Only the curve recorded after 24 hours of exposure stays at almost entire order of magnitude lower current densities (see Fig. 28). The corrosion potential evolves by very peculiar manner. During the initial 2 weeks, it shifts in cathodic direction, and afterwards it comes back towards nobler values. This phenomenon can be explained, proposing that in the

initial period, the coated sample suffers corrosion in the cracks of the coating, and afterwards, the respective corrosion products (such as $\text{Al}(\text{OH})_3$) obstructs the access of corrosive species towards the metallic surface.

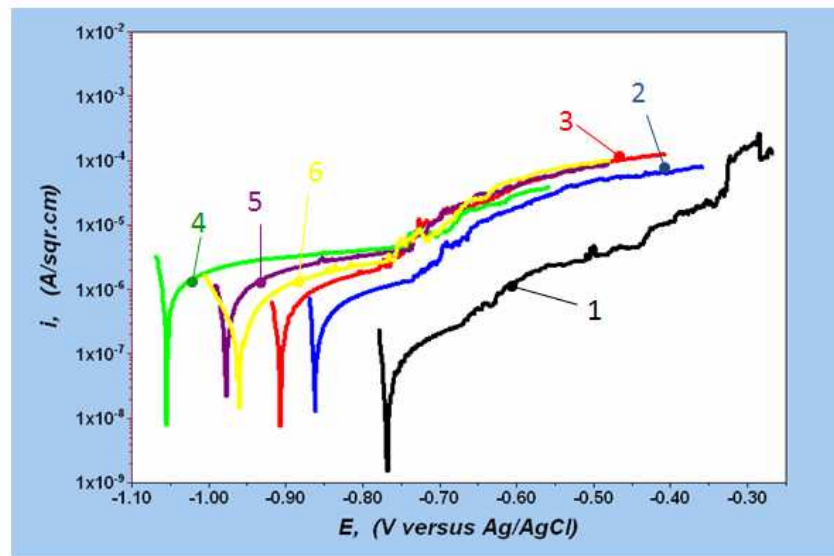


Figure 28. Anodic polarization curves of AA2024 substrate after alkaline preliminary treatment recorded after different exposure times. 1-24h; 2-96h; 3-168h; 4-336h; 5-504h; 6-672h.

The obstruction of the pathways for the corrosive species through a coatings by corrosion products is described in the literature [95, 96]. According to the authors, the obstructions are consequence of formation of aluminium hydroxychloride species, with “Keggin”-like structures, that form semipermeable membranes.

2. Conditions of CeCC depositions:

i. Influence of the concentration of the basic substance of the conversion bath on the features of the CeCC coatings

The optimal concentration of the basic substance, composing the deposition solution was also determined. For that purpose, five metallic substrates, after alkaline preliminary treatment, were submitted to electrodeposition at $-2\text{mA}/\text{cm}^2$, for five minutes. All the deposition solutions were prepared by 10ml. of peroxide. The concentration of the basic ingredient of the coating solution was selected to be: 0.03, 0.04, 0.05, 0.07, 0.10 M, of $(\text{NH}_4)_2\text{Ce}(\text{NO}_3)_5$, respectively as can be seen in figure 29.

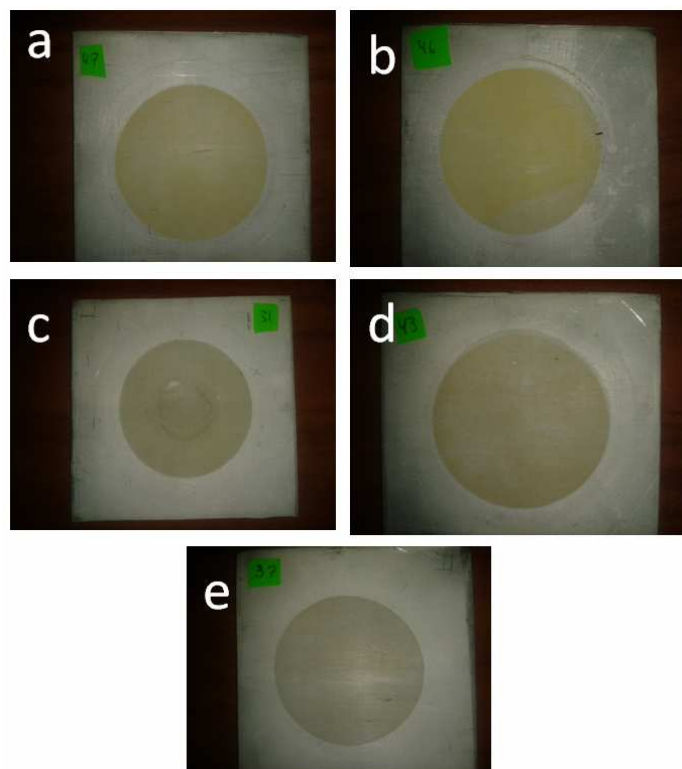


**Fig. 29. Photographs of 5 samples with coatings with different concentration
a – 0.03M; b – 0.04M; c – 0.05M; d – 0.07M; e – 0.1M**

The barrier abilities of the respective coated specimens were examined by electrochemical measurements after 24 hours of exposition to the corrosive medium. The next figure shows the EIS-spectra of the samples.

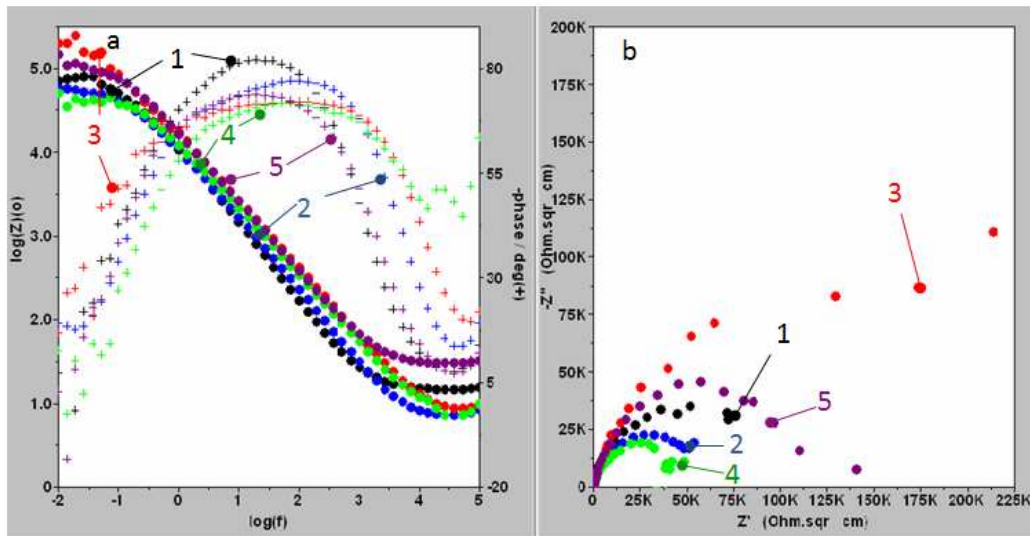


Figure 30. EIS-spectra of samples prepared by CeCC depositions from solutions with different $(\text{NH}_4)_2\text{Ce}(\text{NO}_3)_5$ contents. 1-0.03M; 2-0.04M; 3-0.05M; 4-0.07M; 5-0.1M

The bode plots of the impedance spectra, look almost equal, whereas the Nyquist plots reveal remarkable differences. The largest semi-circle belongs to the sample coated by 0.05 M $(\text{NH}_4)_2\text{Ce}(\text{NO}_3)_5$ solution. Furthermore, its $\log|Z| = f(\log(f))$ – curve at 10 mHz, also has the highest value, revealing that this coating has the best protection ability. The phase shift / $\log(f)$ curves reveal that there are two overlapped maxima, revealing presence of two layers on the metallic surfaces of the samples.

The anodic curves also partially confirm the results, obtained by EIS spectra. Fig. 31 depicts anodic curves, acquired after 24 hours of exposition to model corrosive medium of samples, coated by solutions with different $(\text{NH}_4)_2\text{Ce}(\text{NO}_3)_5$ contents.

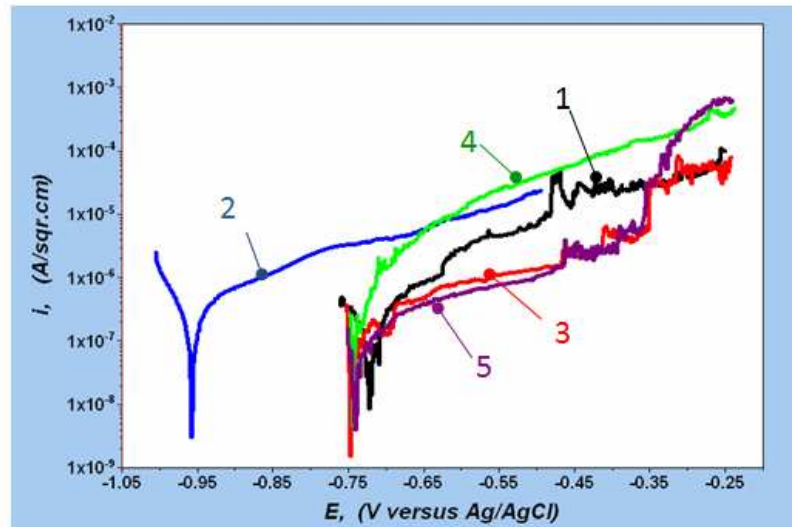


Figure. 31. Anodic polarization curves of AA2024 substrate prepared by CeCC depositions from solutions with different $(\text{NH}_4)_2\text{Ce}(\text{NO}_3)_6$ contents. 1-0.03M; 2-0.04M; 3-0.05M; 4-0.07M; 5-0.1M.

Although the fact that the curve of the best sample, prepared by of 0.05 M $(\text{NH}_4)_2\text{Ce}(\text{NO}_3)_6$ deposition solution, it also reveals clear features of pitting corrosion. Nevertheless, the anodic corrosion current densities of this sample, (together with those, prepared by 0.1 M of the Ce-salt) stay at relatively two orders of magnitude than all of the rest.

As a major result, could be concluded that at different concentrations of $(\text{NH}_4)_2\text{Ce}(\text{NO}_3)_6$ in range 0.01 to 0.1 moles per liter, the optimal composition stays between 0.03 and 0.05 M $(\text{NH}_4)_2\text{Ce}(\text{NO}_3)_6$.

ii. Influence of oxidant addition, and deposition current on the features of the CeCC coatings

In order to investigate the impact of the oxidant addition, entire group of samples was submitted to CeCC deposition, at equal conditions. The metallic substrates were preliminary treated by the procedure for alkaline etching. The depositions were performed for 5 minutes at -2 mA/cm^2 . The basic substance was 0.05 M in the conversion bath solution.

In order to compare the barrier abilities of the coatings, obtained after different additions of H_2O_2 , electrochemical measurements were performed

after 24 hours of exposition to 3.5% NaCl model corrosive medium. Following the literature [80], the increase of the oxidant content should accelerate the coating deposition. Consequently, it is expectable to improve the density, and barrier ability of the coating after increase of H_2O_2 . Nevertheless, it was observed that the elevated content of peroxide, has led to deterioration of the homogeneity and uniformity of the obtained coatings. As could be seen in Fig. 32, all the samples prepared with elevated additions of H_2O_2 have not uniform coatings, but rather they are covered by rough aggregates. Furthermore, these aggregates did not possess almost any adherence to the metallic substrates.

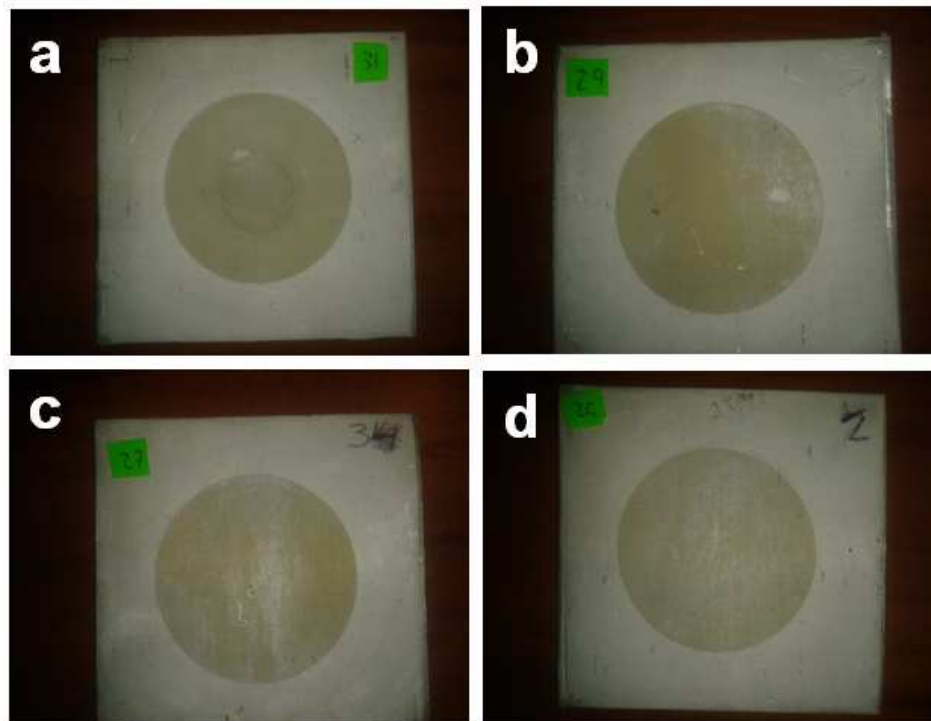


Fig. 32. Photographs of four samples with coatings, deposited after different additions of oxidant

a – 10ml/l addition of H_2O_2 ; b - 25ml/l addition of H_2O_2 ; b - 50ml/l addition of H_2O_2 ; d - 100ml/l addition of H_2O_2 ;

On the figure above, the metallic shining under the Ce-deposits is clearly observable. This fact is obvious evidence of the detrimental effect of the higher H_2O_2 addition.

During the deposition at Galvani-static regime with -2 mA/cm^2 , the equipment was continuously measuring the potentials versus the Ag/AgCl

reference electrode and their evolution within the deposition process. The obtained potential/time diagrams are shown in Fig. 33.

There, after the initial immediate fall of the potential down to almost -1.650 V, the potential reverses its values reaching about -1.300 to -1.350 V. The initial potential drop is related to the current spent for hydrogen evolution on the metallic surface. This process appears due to both of the reducing role of the cathodic current, and the generally acidic character of the deposition solution.

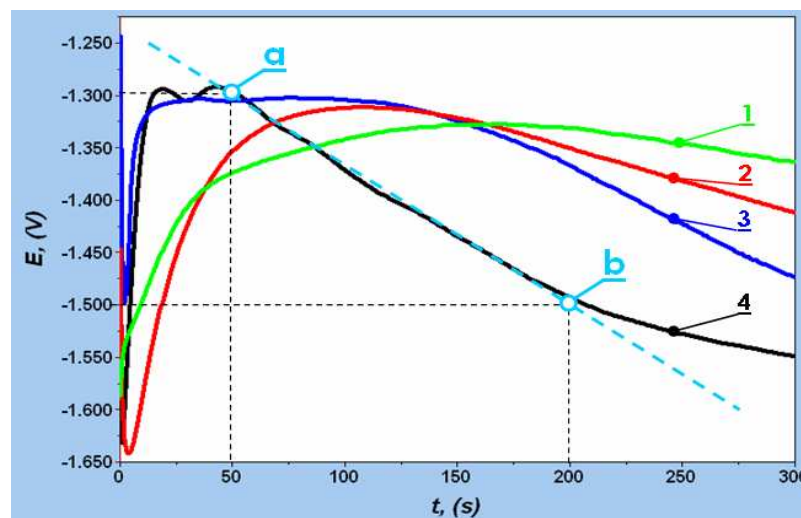


Fig. 33. Chronopotentiometric curves obtained during the Galvani-static depositions of CeCC coatings after different additions of H_2O_2 to the coatings solutions
1 – 100ml/l addition of H_2O_2 ; 2 - 50 – 10ml/l addition of H_2O_2 ; 3 – 25ml/l addition of H_2O_2 ; 4 - 10ml/l addition of H_2O_2

The subsequent reversion of the potential is probably related to removal of the H_2 – gaseous bubbles from the metallic surface. Probably the reason for this removal and the reversion of the potential is the so called “cathodic dissolution of the aluminium”. The most extended continuation is observable for the worst samples – with 100 and 50 ml/l H_2O_2 (175 seconds for curve 1, and 125 seconds for curve 2). The curves 3 and 4 of the samples with more uniform, dense and homogeneous Ce-coatings achieve maxima after 10 - 15 seconds.

After reaching maxima the potentials start to drop gradually again for all curves. This phenomenon is related to either a gradual growth of uniform

coatings (curves 3 and 4), or to occupation of the metallic surface by Cerium containing agglomerates. For the best coating, obtained by addition of only 10 ml/l. H₂O₂, coatings, this gradual drop of potential continued from the 50th (point (a)) to 200th (point (b)) second after the beginning of the deposition. During this time, the potential drops with 200 mV. Taking into account that the deposition is performed in Galvani-static regime (i.e: -2 mA/cm²) and, applying the law of Ohm, it could be calculated that the resistance of the deposited film increases with 100 Ω/cm² for a second. In other words, for the entire period of film growth (between points (a) and (b)) the total resistance of the best film (curve 1) raises up to 15 k Ω/cm². As a general conclusion, it looks that the increase of the H₂O₂ content in the deposition solutions probably favors the cathodic dissolution of the underlying aluminum, hindering the formation of uniform and homogeneous CeCC coatings.

After the depositions, the obtained samples were exposed to 3.5 %NaCl model corrosive media. Their barrier abilities were examined by means of electrochemical measurements techniques (EIS, and LSV). Unexpectedly, the addition of oxidant has not presented its contribution in the impedance spectra. In Fig. 34, all of the spectra possess almost the same shapes, regardless the big difference of the H₂O₂ additions to the solution of the conversion bath.

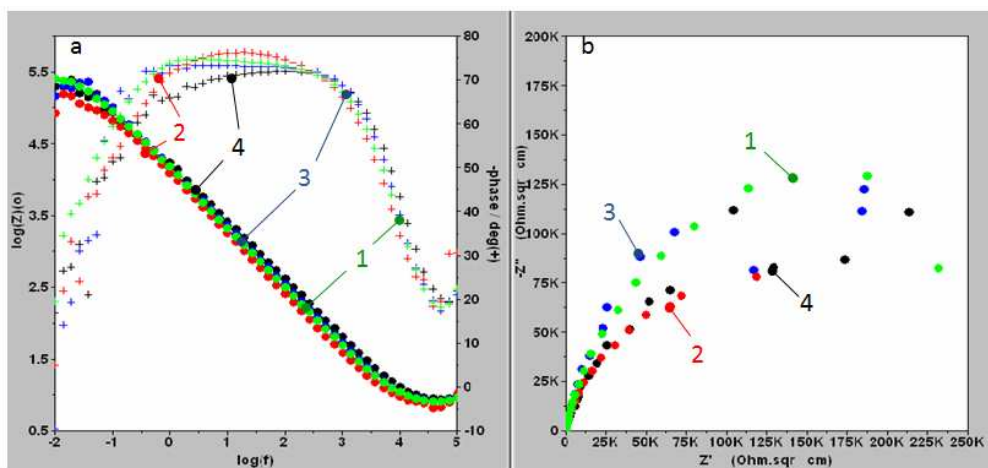


Fig. 34. Electrochemical impedance spectra, acquired after 24 hours of exposition to the model corrosive medium of four specimens coated after different H₂O₂ additions. a – Bode plot; b-Nyquist plot 1 – 100ml/l addition of H₂O₂; 2 - 50 – 10ml/l addition of H₂O₂; 3 – 25ml/l addition of H₂O₂; 4 - 10ml/l addition of H₂O₂

The linear voltammograms reveal more distinguishable features of the respective specimens. Fig. 35 represents Cathodic (a) and anodic (b)

polarization curves recorded after 24 hours of exposition to the model corrosive medium of four specimens coated after different H_2O_2 additions.

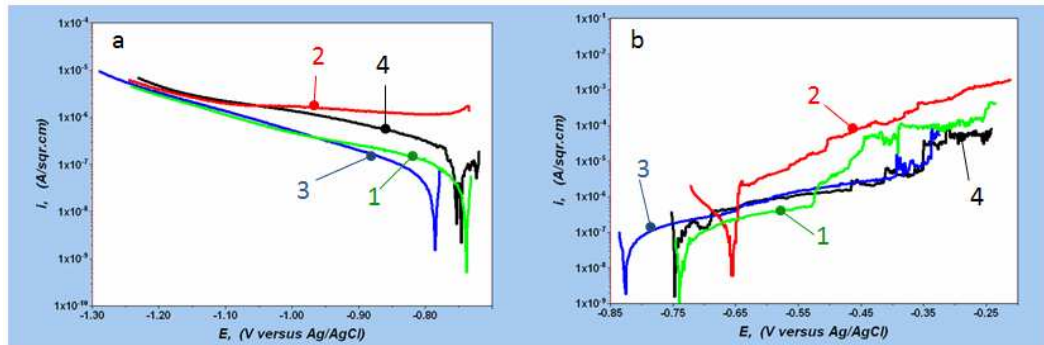


Fig. 35. Cathodic (a) and anodic (b) polarization curves recorded after 24 hours of exposition to the model corrosive medium of four specimens coated after different H_2O_2 additions. 1 – 100ml/l addition of H_2O_2 ; 2 - 50 – 10ml/l addition of H_2O_2 ; 3 – 25ml/l addition of H_2O_2 ; 4 - 10ml/l addition of H_2O_2

All the four samples could be conditionally divided into “better” and “worse”. The former are with relatively lower content of the oxidant (10 and 25 ml. 30% H_2O_2 per liter of coating solution), whereas the latter (50 and 100 ml. 30% H_2O_2 per liter of coating solution).

The worst curves belong to the samples prepared by 50 ml./l. H_2O_2 . Additionally, the respective anodic curve shows a lack of whatever passive region.

Both curves of the sample with 100 ml. H_2O_2 addition stay at lower current densities, than these of the sample coated after 50 ml. H_2O_2 addition.

Nevertheless, the respective anodic curve (of the sample with 50 ml. H_2O_2) has shorter region of passivity (from -750 to -550 mV) than the curves of the samples with lower H_2O_2 additions. According Bethencourt and co. [97], the shorter passivity regions indicate lower strength against pitting nucleation.

Between the “better” samples, the cathodic curve of the sample prepared after 25 ml / l. H_2O_2 stays at lower current densities, than this of the sample with 10 ml. However, the respective anodic curves stay at the same current densities,

revealing very similar barrier ability. Furthermore, the curve of the sample with 10 ml. oxidant addition have relatively larger passivity region.

From these relatively equivocal features of the polarization curves, could be concluded that the optimal addition of peroxide should be in the range of 10 and 25 ml. 30% H₂O₂ for liter of conversion bath.

Another general conclusion that could be done is that because of the application of electric current during the coating deposition, the addition of peroxide as an oxidant is not so important.

For investigation of the influence of the current applied, the electrodepositions were performed at -5 mA/cm². The rest conditions were as described in the previous section (i.e.: alkaline preliminary treatment of the substrates, 0.05 M (NH₄)₂Ce(NO₃)₅ and 10; 25; and 50ml/l H₂O₂). In that manner, the coatings obtained by these conditions could be compared with those, described in the previous section.

Fig. 36 shows four samples with coatings, electrodeposited at -5 mA/cm² after 10, (position (a)), 25 (position (b)), 50, (position (c)) and 100 (position (d)) ml/l. of H₂O₂.

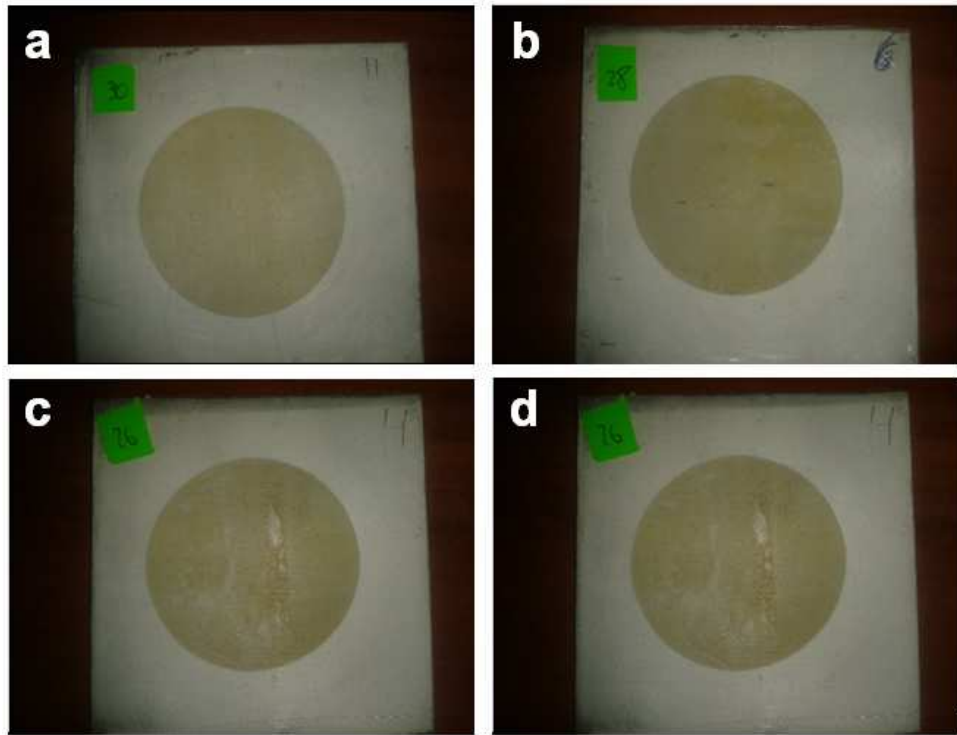


Fig. 36. Photographs of four samples with coatings, deposited after different additions of oxidant
a – 10ml/l addition of H₂O₂; b - 25ml/l addition of H₂O₂; b - 50ml/l addition of H₂O₂; d - 100ml/l addition of H₂O₂;

As could be seen from Fig 36, the samples generally reveal inferior features than those with CeCC electrodeposited at $-2\text{mA}/\text{cm}^2$. Furthermore, the curves, obtained during the electrodeposition do not possess the slope, that should reveal deposition of uniform and homogeneous coating layer (Fig. 37).

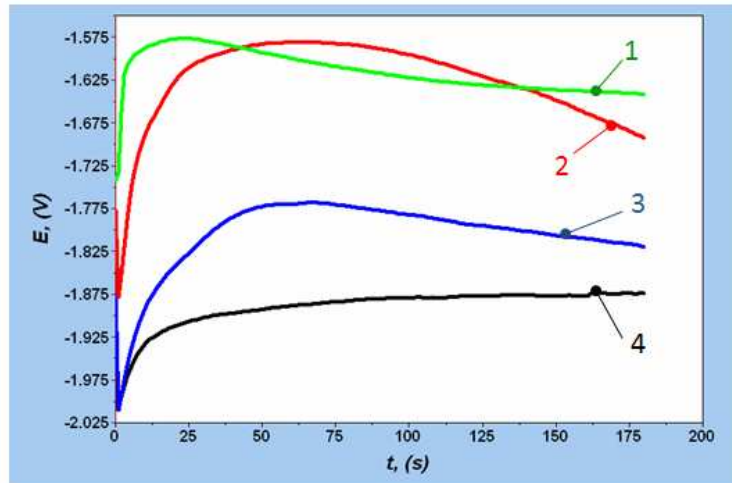


Fig. 37. Chronopotentiometric curves obtained during the Galvani-static depositions of CeCC coatings after different additions of H_2O_2 to the coatings solutions
 1 – 100ml/l addition of H_2O_2 ; 2 - 50 ml/l addition of H_2O_2 ; 3 – 25ml/l addition of H_2O_2 ; 4 - 10ml/l addition of H_2O_2

The barrier abilities of the respective samples were evaluated by electrochemical measurements after 24 hours of exposition to the model corrosive medium, as well. The next figure shows EIS – spectra of the samples with films deposited at -5 mA/cm^2 .

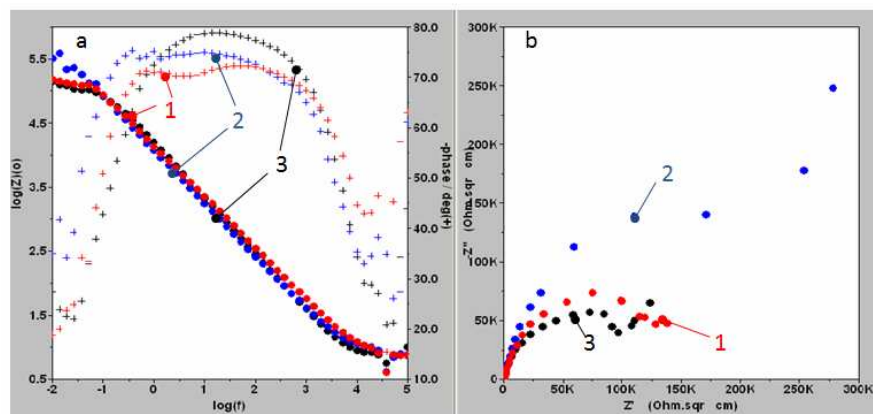


Fig. 38. Electrochemical impedance spectra, acquired after 24 hours of exposition to the model corrosive medium of four specimens coated after different H_2O_2 additions. a – Bode plot; b-Nyquist plot 1 - 50 ml/l addition of H_2O_2 ; 2 – 25ml/l addition of H_2O_2 ; 3 - 10ml/l addition of H_2O_2 .

Here, in the Bode plots, also could not be seen any significant difference among the shapes of the spectra. However, when the Nyquist plots of Figs. 34, and 38 are compared clear Warburg diffusion elements are observable in the latter figure (i.e: samples with 5 mA/cm² deposition current density). This fact evidences that the higher deposition currents applied result in formation of rather less uniform deposits. Indeed, the visual inspections of the samples revealed rough and grain-formed (agglomerates) coatings, when the higher current was used. The unsatisfying homogeneity of the coatings favors the access of corrosive species to the metallic surface, resulting in appearance of the Warburg impedance.

Fig. 39 reveals that there are lower differences among the polarization curves of the samples prepared with different H₂O₂ additions, compared to those, in Fig. 35.

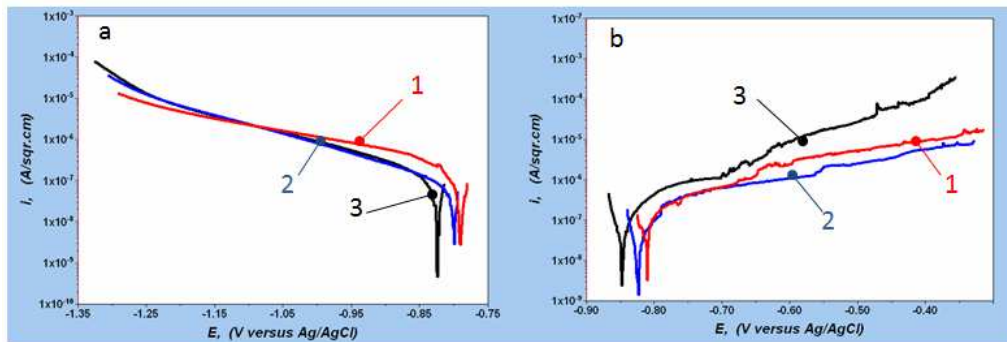


Fig. 39. Cathodic (a) and anodic (b) polarization curves recorded after 24 hours of exposition to the model corrosive medium of four specimens coated after different H₂O₂ additions. 1 - 50 ml/l addition of H₂O₂; 2 - 25ml/l addition of H₂O₂; 3 - 10ml/l addition of H₂O₂.

This phenomenon could be easily explained, because the deposition current plays a role of reducer. As a result, at higher current densities (-5mA/cm²), the influence of the H₂O₂ as oxidant is less notable. The supply of electrons towards the specimen (by the electric current) leads to deactivation of the peroxide by obtaining of OH⁻ ions (see equation 2 of the literature review) and acceleration of oxygen reduction (see equation 4 of the literature review). Both these processes result in alkalisation of the medium near the substrate surface and acceleration of Ce-precipitation (see equation 3).

However, the obtained Ce(OH)₃/Ce(OH)₄ precipitates do not form a coating layer, but rather conjunction of clusters.

iii. Superficial morphologic observations

In order to observe the morphology of the coated samples, Optical Metallographic Microscopy (OMM) and Scanning Electronic Microscopy (SEM), combined by energy dispersion X-ray analysis were applied on the best samples before and after 168 hours of exposition to naturally aerated 3.5% NaCl model corrosive medium. OMM images are shown in the figure below. The samples that have shown the best results (Highest barrier ability and durability) were submitted to OMM and SEM. They are prepared by the following conditions: **(i)** – Deposition at 0.03M $(\text{NH}_4)_2\text{Ce}(\text{NO}_3)_5$ with 10ml/L H_2O_2 , $2\text{mA}/\text{cm}^2$ for 7 minutes (a,b); **(ii)** - Deposition at 0.05M $(\text{NH}_4)_2\text{Ce}(\text{NO}_3)_5$ with 10ml/L H_2O_2 , $2\text{mA}/\text{cm}^2$ for 7 minutes (c,d); **(iii)** - Deposition at 0.05M $(\text{NH}_4)_2\text{Ce}(\text{NO}_3)_5$ with 10ml/L H_2O_2 , $2\text{mA}/\text{cm}^2$ for 5 minutes (e,f)

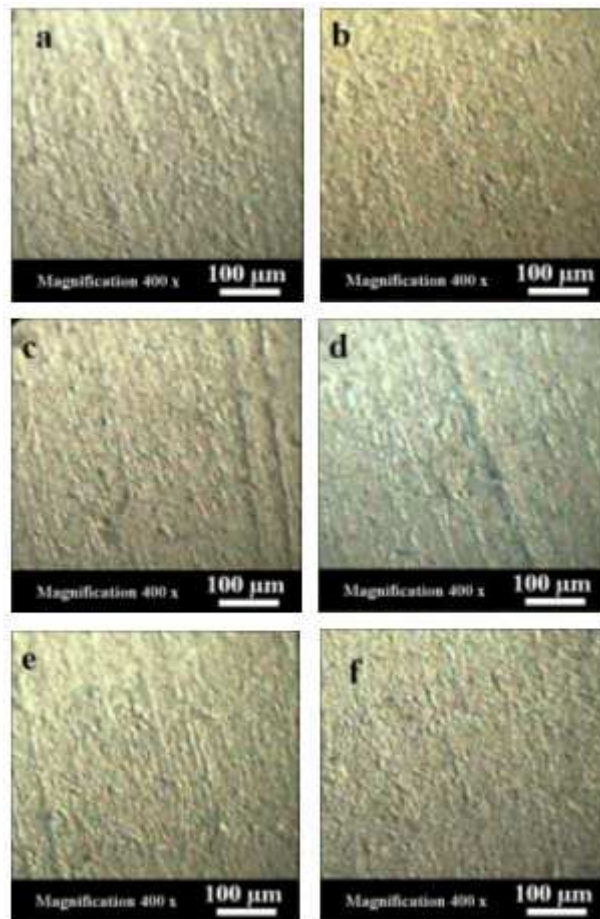


Fig 40. OMM images of the best samples before (a,c,e), and after 168h. of exposure to the model corrosive medium (b,d,f).

To follow how the surfaces of the metallic specimens change after the CeCC electrodeposition, and what is the level of coverage by the coatings,

several SEM observations combined by EDX elemental analyses were performed. The next figure represents SEM image of metallic substrate after mechanical and alkaline treatment. Clear furrows as traces of the emery papers are observable on the metallic surface.

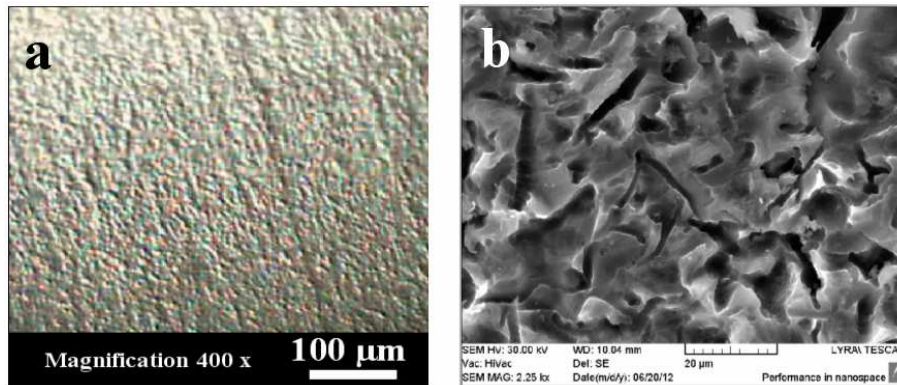


Fig. 41. OMM (a) and SEM (b) – images of AA2024 metallic substrate after mechanical and alkaline treatments

Superficial SEM / EDX characterizations on coated samples were done, as well. The next figure shows the surface images, obtained by SEM of two samples coated by electrodeposition for 5 or 7 minutes from 0.05M $(\text{NH}_4)_2\text{Ce}(\text{NO}_3)_5$ with 10ml/l addition of H_2O_2 after mechanical + alkaline pre-treatment.

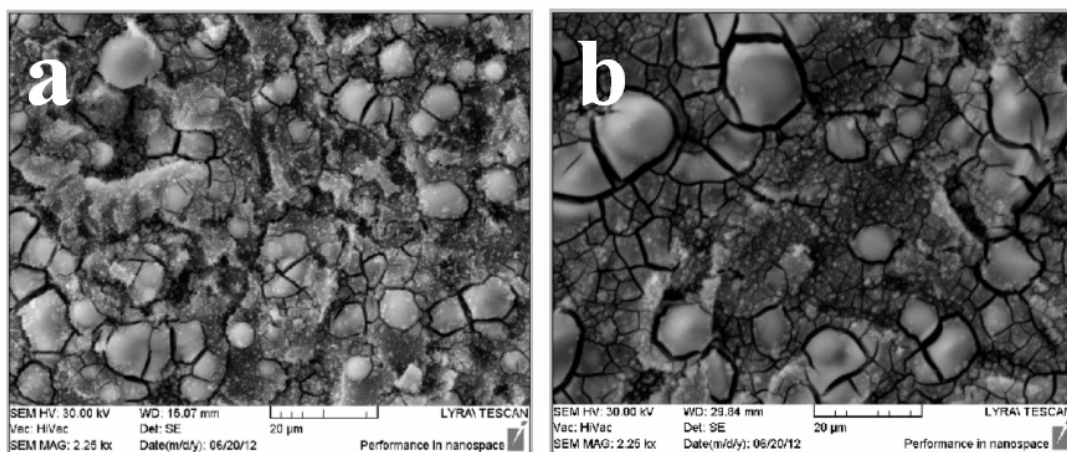


Fig. 42. SEM images of two samples with electrodeposited coatings

A – after 5 minutes of electrodeposition; b – after 7 minutes of electrodeposition

As could be seen from the figure, the continuation of the electrodeposition does not lead to any changes of surface morphology. After 5

minutes (position (a)), the sample looks completely covered by the coating layer. The comparison between Figs. 41 and 42 reveals completely different surfaces, indicating that the coating has completely covered the metallic surface. In addition, there is not any difference between the images in positions (a) and (b). Another interesting feature of these coatings is that they possess peculiar features. Larger oval hills are clearly distinguishable on the surfaces. Probably these sides are locations of preferential deposition of the layer, as was observed in previous works [98]. Consequently, these oval hills are formed as consequence of preferential deposition on intermetallics.

After 168 hours of exposure to model corrosive medium, any remarkable changes were observed, as could be seen in the next figure.

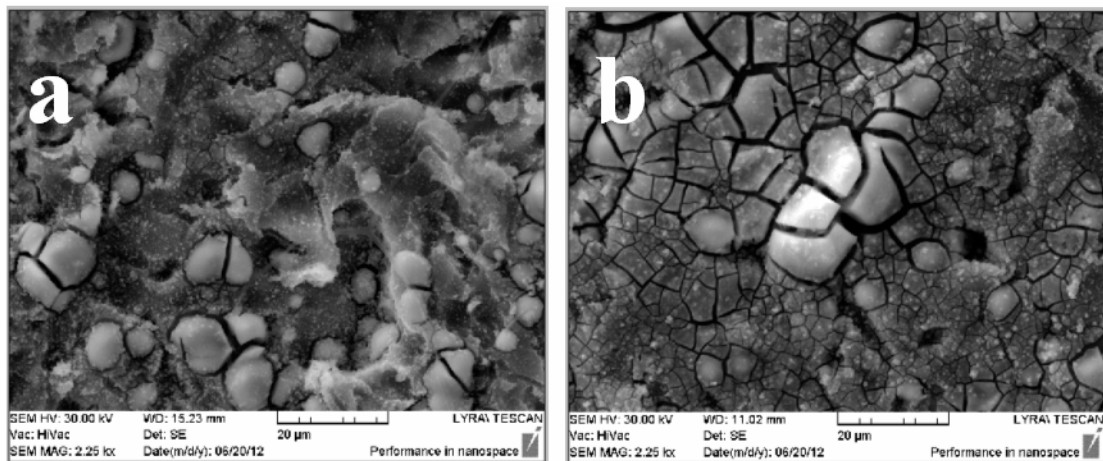


Fig. 43. SEM images of two samples with electrodeposited coatings

A – after 5 minutes of electrodeposition; b – after 7 minutes of electrodeposition

The samples prepared by deposition for 7 minutes from 0.03 M $(\text{NH}_4)_2\text{Ce}(\text{NO}_3)_5$ with 10ml/l addition of H_2O_2 after mechanical + alkaline pre-treatment show almost the same superficial morphology as the previous. The following figure shows two images of sample, prepared by these conditions, before (position (a)) and after 168 hours of exposition (position (b)) to 3.5% NaCl corrosive medium.

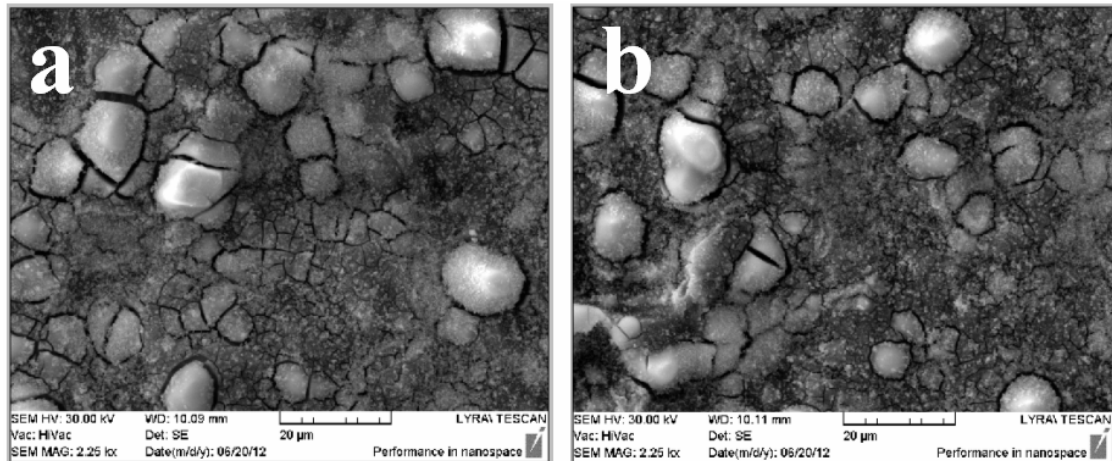


Fig. 44. SEM Images of sample, prepared by these conditions, before (position (a)) and after 168 hours of exposition to 3.5% NaCl corrosive medium.

- *EDX analysis* – In order to clarify the real composition of the samples, and the distribution of the elements on their surfaces, EDX – map analyses were executed during the SEM observations. The next figure represents the elemental distributions of the most important chemical elements: Al, Ce, Cu, and oxygen. These elements were selected because the aluminium could be presented not only from the metallic substrate, but also to compose corrosion products, in form of $\text{Al}(\text{OH})_3$, etc. The cerium was selected because this element together with the oxygen are the basic components of the coating. The copper was also selected to be monitored, because it should reveal whether the S-phases are preferable locations of deposition, and is there a copper re-deposition as evidence of corrosion during the deposition. The next figure shows EDX –map data of the SEM image in Fig. 45.

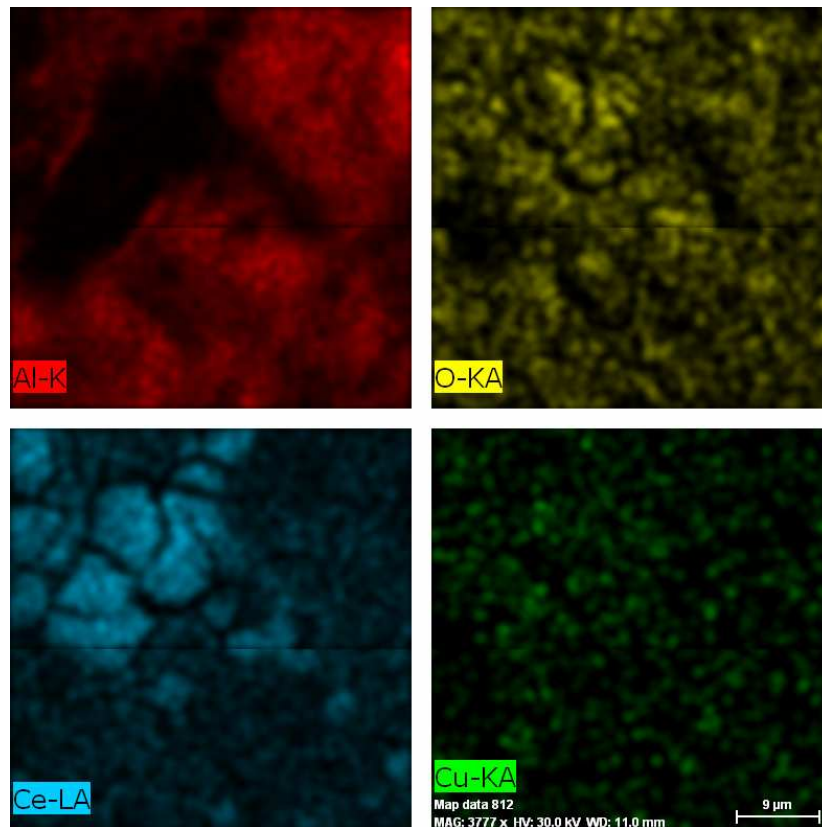


Fig. 45. EDX map data of sample after prepared by deposition for 7 minutes from 0.03 M $(\text{NH}_4)_2\text{Ce}(\text{NO}_3)_5$ with 10ml/l addition of H_2O_2 after mechanical + alkaline pre-treatment

When position (b) of figure 43 and the Al-distribution map of Fig. 45 are compared, could be concluded that there is aluminium deposited on the coating. It is undoubtedly originated from corrosion products formed during the deposition. The map of cerium shows that the sides of preferable deposits coincide with the highest abundance of cerium. Nevertheless, there is uniform distribution of this element on the rest part of the coated surface. The copper is also equally distributed on the metallic surface. This fact is consequence and indication of copper re-distribution. This process passes because of the cathodic Al-dissolution of the metallic matrix.

Similar map-analyses were performed after 168 hours exposition to corrosive medium, as well. Fig. 46. EDX map data of sample after prepared by deposition for 7 minutes from 0.03 M $(\text{NH}_4)_2\text{Ce}(\text{NO}_3)_5$ with 10ml/l addition of H_2O_2 after mechanical + alkaline pre-treatment and subsequent exposition naturally aerated 3.5% NaCl model corrosive medium.

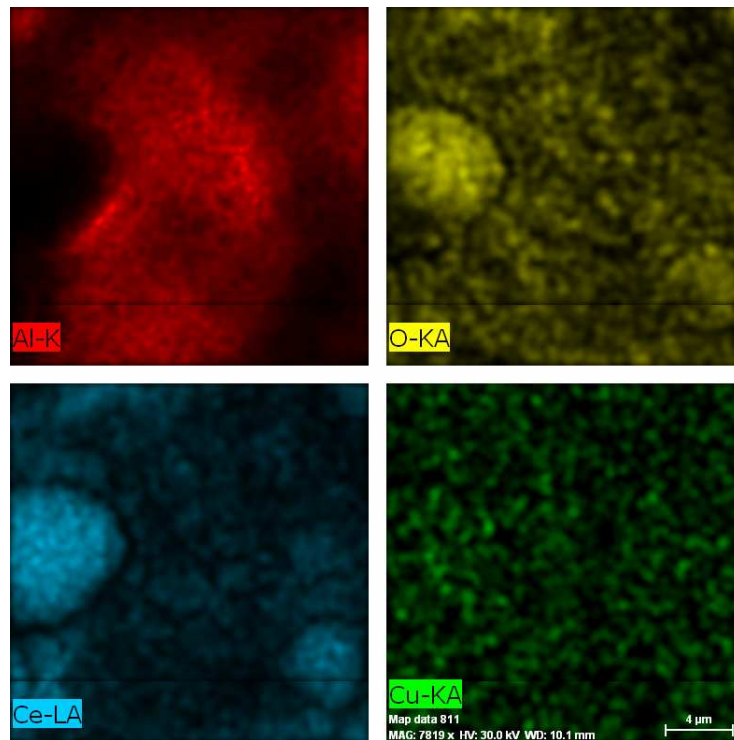


Fig. 46. EDX map data of sample after prepared by deposition for 7 minutes from 0.03 M $(\text{NH}_4)_2\text{Ce}(\text{NO}_3)_5$ with 10ml/l addition of H_2O_2 after mechanical + alkaline pre-treatment

The exposition to corrosive medium did not led to significant changes of the superficial composition and element distribution. All of the selected elements (i.e.: Al, O, Ce and Cu) reveal the same features as described for Fig. 45. The same situation is observed for the sample coated by 0.05 M solution of the cerium compound, at the same conditions.

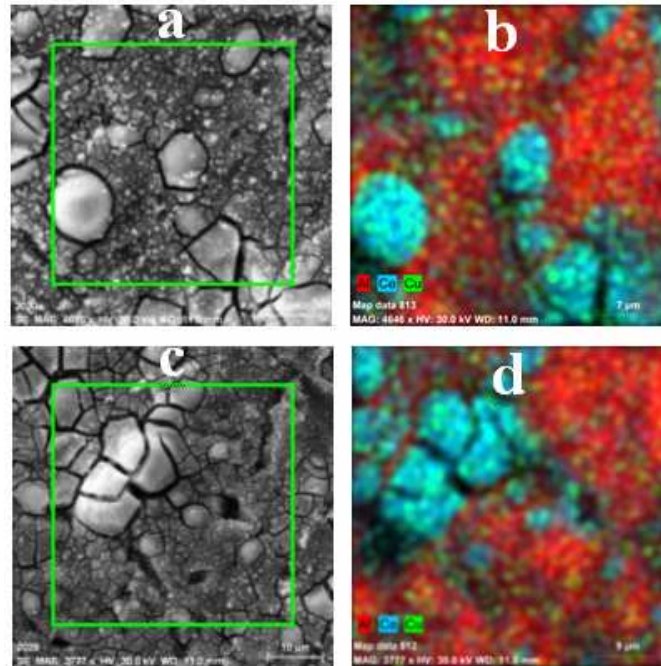


Fig. 47. SEM images (a, c) and EDX map data (b, d) of intact coating (a, b) and submitted to corrosion area (c, d) of sample coated for 7 minutes by 0.05 M solution

In order to clarify the compositions of the bright and dark zones, quantitative point analyses were performed on them. Fig. 47 shows two point analyses on a bright (positions a and c) and dark (positions b and d) areas of a CeCC coating, electrodeposited for 7 minutes on a substrate after mechanical + alkaline treatments. The solution for electrodeposition was performed in 0.05 M $(\text{NH}_4)_2\text{Ce}(\text{NO}_3)_6$ with 10ml/l. H_2O_2 and subsequent submission to 3.5% NaCl.

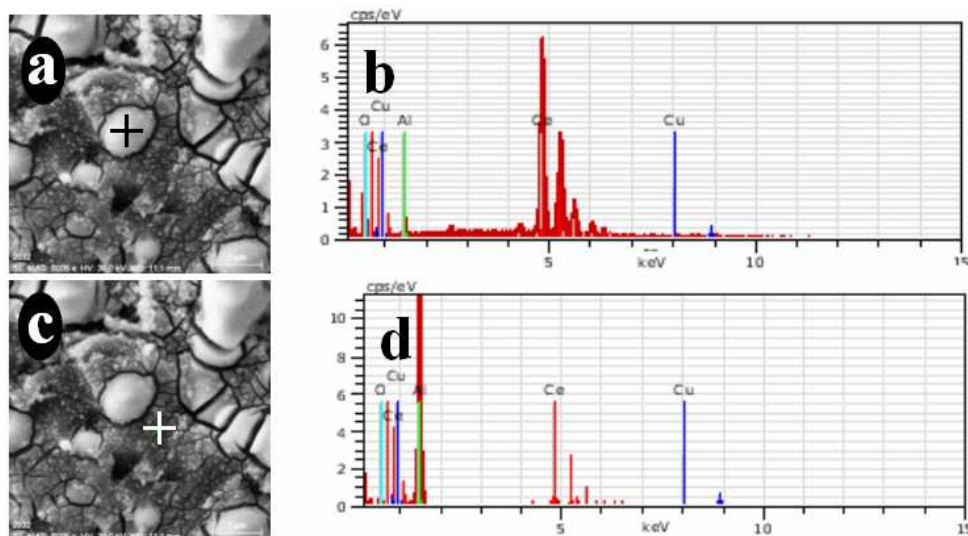


Fig. 48. SEM images (a, c) and EDX point analyses (b, d) of bright and dark zones of a coating after 168 hours of exposure to 3.5% NaCl solution

After the execution of these analyses was concluded that the bright areas contain more than 90 % at. Ce, whereas in the darker zones, the Ce-coating is covered or mixed with Al-containing corrosion products. This fact could be seen from the next tables.

Table 5. Elemental composition determined by the point analysis of the bright point of the coating

El	AN	Series	unn. C [wt.%]	norm. C [wt.%]	Atom. C [at.%]	Error [%]
O	8	K-series	30.72	32.61	76.55	4.4
Ce	58	L-series	58.42	62.00	16.62	1.6
Al	13	K-series	4.28	4.54	6.32	0.3
Cu	29	K-series	0.81	0.86	0.51	0.1
Total:			94.23	100.00	100.00	

As could be seen on the table above, the atomic concentration Ce is almost three times higher than this of the aluminium. Surprisingly, there is unexpectedly low content of copper. This fact could be explained, taking in account that may be the intermetallics are completely covered by rather thick Ce-layer.

In the dark zone, more than 62 atomic units belong to Al, and only traces of Ce are represented (see the table below).

Table 6. Elemental composition determined by the point analysis of the dark point of the coating

El	AN	Series	unn. C [wt.%]	norm. C [wt.%]	Atom. C [at.%]	Error [%]
Al	13	K-series	61.53	69.61	62.54	3.1
O	8	K-series	21.15	23.93	36.26	3.2
Ce	58	L-series	5.40	6.11	1.06	0.2
Cu	29	K-series	0.31	0.36	0.14	0.0
Total:			88.39	100.00	100.00	

Comparing the tabular data for the dark and bright zones, could be concluded that the coatings are not enough homogeneous, but they are rather represented by mixture of Ceoxides/hydroxides, surrounded by Al-corrosion products, deposited on the coating, or mixed with the Ce-layer.

V. CONCLUSIONS

1. Diammonium pentanitrocerate was used as provider of Ce-ions during the coating deposition. In this substance, the Ce is presented in the anionic compositional part in difference of the Ce-substances described in the World wide literature, until nowadays.

2. It is established that the samples with the best barrier ability, adherence, and uniformity were achieved after alkaline preliminary treatment, compared to the mechanical and acidic approaches.

3. It is found that at different concentrations of $(\text{NH}_4)_2\text{Ce}(\text{NO}_3)_5$ in range 0.01 to 0.1 moles per liter, the optimal concentration is between 0.03 and 0.05 M $(\text{NH}_4)_2\text{Ce}(\text{NO}_3)_5$.

4. It is determined that the optimal content of peroxide is in the range of 10 and 25 ml/l. of 30% H_2O_2 .

5. It is established that the best Conversion Coatings were obtained at $i=2\text{mA/cm}^2$ current density and 5 minutes time deposition

6. It was determined by SEM and OMM observations that the morphology of the coating does not repeat the one of the metallic substrate, showing complete coverage by the coating.

7. The Cerium conversion coatings elaborated in the present research work could serve as a basis of future coating systems

VI. REFERENCES

1. <http://www.iso.org/iso/home.html>
2. <http://asm.matweb.com/search/SpecificMaterial.asp?bassnum=MA2024T4>
3. http://www.splav.kharkov.com/en/e_mat_start.php?name_id=1438
4. http://www.alu.com.cn/enCompany/ShowPro_3367_dflc.html

5. Frederico M. Mazzolani “**Aluminium alloy structures**” *E& FN SPON ed. Second edition (1985) pp. 5 – 25*
6. http://www.kaiseraluminum.com/wp-content/themes/kac/files/alloy-pdfs/2024_Rod_Bar.pdf
7. <http://www.suppliersonline.com/propertypages/2024.asp>
8. http://www.asminternational.org/content/ASM/StoreFiles/06691G_Chapter_1.pdf
9. Autolab instruments are developed and produced by metrohm autolab B.V. in the Netherlands, accessible by www.metrohm-autolab.com
10. E. Matter, S. Kozhukharov, “*Correlation between preliminary pretreatments and the behaviour of AA-2024 – aluminium alloy in 3.5% NaCl model corrosive medium*” Annual reports of “Angel Kanchev” University of Ruse (Razgrad) **2010**
11. D. Zhao, J. Sun, L. Zhang, Y. Tan, J. Li “*Corrosion behavior of rare earth cerium based conversion coating on aluminum alloy*” JOURNAL OF RARE EARTHS, **28**, (2010). 371 -374
12. Rangel C M, Paiva T L, Daluz P P. “*Anticorrosion treatments for aluminum and aluminum alloys. European Symposium on Corrosion Inhibitor*”, 2000, **29(9)**: 507.
13. Bethencourt M, Botana F J, Cano M J. “*High protective, environmental friendly and short-time developed conversion coatings for aluminum alloys*”. Applied Surface Science, 2002, **189(1/2)**: 162.
14. Z. Nenova, S. Ivanov, T. Nenov “Sensors in industrial automation” Ed. EKS-PRES (Gabrovo), 2011, pp. 95 (In Bulgarian).
15. W. Pinc, S. Geng, M. O’Keefe, W. Fahrenholtz, T. O’Keefe “*Effects of acid and alkaline based surface preparations on spray deposited cerium based conversion coatings on Al 2024-T3*” Appl. Surf. Sci. **255** (2009) 4061–4065
16. C. Girginov, S. Kozhukharov “*Surface of Alumina Films after Prolonged Breakdowns in Galvanostatic Anodization*” International Journal of Electrochemistry ID 126726 (2012) 5p.
17. K. Srinivasa Rao and K. Prasad Rao, “*Pitting corrosion of heat-treatable aluminium alloys and welds: a review*”, Trans. Indian Inst. Met, **57**, (6), (2004) 593-610.

18. K.A. Yasakau, M.L. Zheludkevich, S.V. Lamaka and M.G.S. Ferreira, “*Mechanism of Corrosion Inhibition of AA2024 by Rare-Earth Compounds*”, J. Phys. Chem. B, **110** (2006) pp. 5515 – 5528
19. J.G. Brunner, N. Birbilis, K.D. Ralston, S. Virtanen, “*Impact of ultrafine-grained microstructure on the corrosion of aluminium alloy AA2024*”, Corrosion Science **57** (2012) 209–214
20. K.D. Ralston, D. Fabijanic, N. Birbilis, “*Effect of grain size on corrosion of high purity aluminium*”, Electrochim. Acta **56** (2011) 1729–1736.
21. E. Kus, Z. Lee, S. Nutt, F. Mansfeld, “*A comparison of the behavior of nanocrystalline and conventional Al 5083 samples*”, Corrosion **62** (2006) 152–161.
22. E. Sikora, X.J. Wei, B.A. Shaw, “*Corrosion behavior of nanocrystalline bulk Al–Mg-based alloys*”, Corrosion **60** (2006) 387–398.
23. T.C. Tsai, T.H. Chuang, “*Role of grain size on the stress corrosion cracking of 7475 aluminum alloys*”, Mater. Sci. Eng., A **225** (1997) 135–144.
24. I.J. Son, H. Nakano, S. Oue, S. Kobayashi, H. Fukushima, Z. Horita, “*Pitting corrosion resistance of ultra-fine grained Aluminium processed by Severe Plastic Deformation*”, Mater. Trans. **47** (2006) 1163–1169.
25. M.K. Chung, Y.S. Choi, J.G. Kim, Y.M. Kim, J.C. Lee, “*Effect of the number of ECAP pass time on the electrochemical properties of 1050 Al alloys*”, Mater. Sci. Eng. A **366** (2004) 282–291.
26. M. Hockauf, L.W. Meyer, D. Nickel, G. Alisch, T. Lampke, B. Wielage, L. Krueger, “*Mechanical properties and corrosion behaviour of ultrafine-grained AA6082 produced by equal-channel angular pressing*”, J. Mater. Sci. **43** (2008) 7409–7417.
27. K.D. Ralston, J.G. Brunner, S. Virtanen, N. Birbilis, “*Effect of processing on grain size and corrosion of AA 2024-T3*”, Corrosion **67** (2011) (art. no. 105001).
28. Karl-Heinz Haas, Klaus Rose, “*Hybrid inorganic/organic polymers with nanoscale building blocks: precursors, processing*,” Rev. Adv. Mater. Sci. **5** (2003) 47–52

29. G. Tsaneva, V. Kozhukharov, S. Kozhukharova, M. Ivanova, J. Gerwann, M. Schem, T. Schmidt, “*Functional nanocomposite coatings for corrosion protection of aluminium alloy and steel*”, Journal of the University of Chemical Technologies and Metallurgy **43** (2) (2008) 231 - 238
30. J. Zhao, L. Xia, A. Sehgal, D. Lu, R.L. McCreery, G.S. Frankel, “*Effects of chromate and chromate conversion coatings on corrosion of aluminum alloy 2024-T3*”, Surface and Coatings Technology, **140** (2001) 51 – 57
31. J.V. Kloet, W. Schmidt, A.W. Hassel, M. Stratmann, *The role of chromate in filiform corrosion inhibition*, Electrochimica Acta, **49** (2004) 1675 – 1685
32. S. John, “*Challenges of chromate inhibitor pigments replacement in organic coatings*”, Progress in Organic Coatings, **42** (2001) 267 – 282
33. J.D. Ramsey, R.L. McCreery, “*Raman microscopy of chromate interactions with corroding aluminum alloy 2024-T3*”, Corrosion Science, **46** (2004) 1729 – 1739
34. V.I. Pokhmurskii, I.M. Zin, V.A. Vynar, L.M. Bily, “*Contradictory effect of chromate inhibitor on corrosive wear of aluminium alloy*” Corrosion Science, **53** (2011) 904 – 908
35. A. Foyet, T.H. Wu, A. Kodentsov, L. van der Ven, G. de With, R. van Bentem, “*Impedance evaluation of permeability and corrosion of Al-2024 aluminum alloy coated with a chromate free primer*” Progress in Organic Coatings, **65** (2009) 257 – 262
36. M. Kendig, S. Jeanjaquet, R. Addison, J. Waldrop, *Role of hexavalent chromium in the inhibition of corrosion of aluminum alloys*, Surface and Coatings Technology, **140** (2001) 58 – 66

37. S.A. Katz, H. Salem, *The Biological and Environmental Chemistry of Chromium*, VCH Publishers, New York, (1994).
38. M. Costa, C. Klein, Toxicity and carcinogenicity of chromium compounds in humans, *Crit Rev Toxicol*, 2 (2006) 155-163.
39. Directive 2004/107/EC of the European Parliament and of the Council of 15 December 2004 relating to arsenic, cadmium, mercury, nickel and polycyclic aromatic hydrocarbons in ambient air. Official Journal of the European Communities L 23, 26.1.2005, p. 3–16, Special edition in Bulgarian: Chapter 15 Volume 13 P. 124 – 137
40. EU Directive 2002/95/EC “*Restriction of Hazardous Substances in Electrical and Electronic Equipment*” (RoHS directive 2002), www.broadcom.com/docs/ и www.chem.agilent.com/
41. White paper COM (2001)88 final on the strategy for a future Chemicals Policy, 16-2-2001
42. CEPE, *Best Available Techniques for Coatings Manufacture*; <http://www.cepe.org>
43. N. Greenwood and A. Earnshaw, *Chemistry of Elements* (Pergamon press, Oxford, England, - 1984), p. 1437.
44. T.J. Haley, *J. Pharm. Sci.*, **54** (1965) 633.
45. DHHS-NIOSH, REGISTRY OF TOXIC EFFECTS OF CHEMICAL SUBSTANCES in, DHHS-NIOSH, 1986, pp. 103.
46. P.J. Falconnet, “*The rare earth industry: a world of rapid change*”, *Journal of Alloys and Compounds*, **192** (1993) 114 – 117

47. N.C. Rosero-Navarro, M. Curioni, R. Bingham, A. Durán, M. Aparicio, R.A. Cottis, G.E. Thompson, “*Electrochemical techniques for practical evaluation of corrosion inhibitor effectiveness. Performance of cerium nitrate as corrosion inhibitor for AA2024T3 alloy*”, Corrosion Science, **52** (2010) 3356 – 3366
48. P.A. White, A.E. Hughes, S.A. Furman, N. Sherman, P.A. Corrigan, M.A. Glenn, D. Lau, S.G. Hardin, T.G. Harvey, J. Mardel, T.H. Muster, S.J. Garcia, C. Kwakernaak, J.M.C. Mol, “*High-throughput channel arrays for inhibitor testing: Proof of concept for AA2024-T3*”, Corrosion Science, **51** (2009) 2279 – 2290
49. L.S. Kasten, J.T. Grant, N. Grebasch, N. Voevodin, F.E. Arnold, M.S. Donley, “*An XPS study of cerium dopants in sol-gel coatings for aluminum 2024-T3*”, Surface and Coatings Technology, **140** (2001) 11 – 15
50. M.L. Zheludkevich, R. Serra, M.F. Montemor, K.A. Yasakau, I.M.M. Salvado, M.G.S. Ferreira, “*Nanostructured sol-gel coatings doped with cerium nitrate as pre-treatments for AA2024-T3: Corrosion protection performance*”, Electrochimica Acta, **51** (2005) 208 – 217
51. M.A. Arenas, M. Bethencourt, F.J. Botana, J. de Damborenea, M. Marcos, “*Inhibition of 5083 aluminium alloy and galvanised steel by lanthanide salts*”, Corrosion Science, **43** (2001) 157 – 170
52. K.A. Yasakau, M.L. Zheludkevich, M.G.S. Ferreira, “*Lanthanide Salts as Corrosion Inhibitors for AA5083. Mechanism and Efficiency of Corrosion Inhibition*”, J. Electrochem. Soc., **155** (2008) C169 - C177
53. H. Allachi, F. Chaouket, K. Draoui, “*Protection against corrosion in marine environments of AA6060 aluminium alloy by cerium chlorides*”, Journal of Alloys and Compounds, **491** (2010) 223 – 229

54. B. Davó, J.J. de Damborenea, “*Use of rare earth salts as electrochemical corrosion inhibitors for an Al-Li-Cu (8090) alloy in 3.56% NaCl*”, *Electrochimica Acta*, **49** (2004) 4957 – 4965
55. A. Aballe, M. Bethencourt, F.J. Botana, M. Marcos, “*CeCl₃ and LaCl₃ binary solutions as environment-friendly corrosion inhibitors of AA5083 Al-Mg alloy in NaCl solutions*”, *Journal of Alloys and Compounds*, **323-324** (2001) 855 – 858
56. S. Kozhukharov, V. Kozhukharov, M. Wittmar, M. Schem, M. Aslan, H. Caparrotti, M. Veith, “*Protective abilities of nanocomposite coatings containing Al₂O₃ nanoparticles loaded by CeCl₃*”, *Progress in Organic Coatings*, **71** (2011) 198 – 205
57. S.J. García, T.H. Muster, Ö. Özkanat, N. Sherman, A.E. Hughes, H. Terryn, J.H.W. de Wit, J.M.C. Mol, “*The influence of pH on corrosion inhibitor selection for 2024-T3 aluminium alloy assessed by high-throughput multielectrode and potentiodynamic testing*”, *Electrochimica Acta*, **55** (2010) 2457 – 2465
58. S. Kozhukharov, V. Kozhukharov, M. Wittmar, M. Schem, M. Aslan, H. Caparrotti, M. Veith, “*Protective abilities of nanocomposite coatings containing Al₂O₃ nanoparticles loaded by CeCl₃*”, *Progress in Organic Coatings*, **71** (2011) 198 – 205
59. A.K. Bhattamishra, M.K. Banerjee, “*Corrosion behavior of Al-Zn-Mg alloys in NaCl solution in presence of cerium salts*”, *Zeitschrift für metallkunde*, **84** (1993) 734 – 736
60. D. Ho, N. Brack, J. Scully, T. Markley, M. Forsyth, B. Hinton, “*Cerium Dibutylphosphate as a Corrosion Inhibitor for AA2024-T3 Aluminum Alloys*”, *J. Electrochem. Soc.*, **153** (2006) B392 - B401
61. P.A. White, A.E. Hughes, S.A. Furman, N. Sherman, P.A. Corrigan, M.A. Glenn, D. Lau, S.G. Hardin, T.G. Harvey, J. Mardel, T.H. Muster, S.J. Garcia, C. Kwakernaak,

- J.M.C. Mol, “*High-throughput channel arrays for inhibitor testing: Proof of concept for AA2024-T3*”, Corrosion Science, **51** (2009) 2279 – 2290
62. N. Birbilis, R.G. Buchheit, D.L. Ho, M. Forsyth, “*Inhibition of AA2024-T3 on a phase-by-phase basis using an environmentally benign inhibitor, cerium dibutyl phosphate*”, Electrochemical and solid-state letters, **8** (2005) C180-C183.
63. J. Mardel, S.J. Garcia, P.A. Corrigan, T. Markley, A.E. Hughes, T.H. Muster, D. Lau, T.G. Harvey, A.M. Glenn, P.A. White, S.G. Hardin, C. Luo, X. Zhou, G.E. Thompson, J.M.C. Mol, “*The characterisation and performance of Ce(dbp)₃-inhibited epoxy coatings*”, Progress in Organic Coatings, **70** (2011) 91 - 101.
64. E. Hughes, D. Ho, M. Forsyth, B.R.W. Hinton, “*Rare earth inhibited systems,*” Proceed. Tri-Service Corrosion Conference Nov. 14-18, Orlando, FL 2005, pp. 1-10.
65. M. Forsyth, T. Markley, D. Ho, G.B. Deacon, P. Junk, B. Hinton, A.E. Hughes, “*Inhibition of corrosion on AA2024-t3 by new environmentally friendly rare earth organophosphate compounds*” Corrosion, **64** (2008) 191 – 197
66. J.-A. Hill, T. Markley, M. Forsyth, P.C. Howlett, B.R.W. Hinton, “*Corrosion inhibition of 7000 series aluminium alloys with cerium diphenyl phosphate*”, Journal of Alloys and Compounds, **509** (2011) 1683 – 1690
67. T.A. Markley, M. Forsyth, A.E. Hughes, “*Corrosion protection of AA2024-T3 using rare earth diphenyl phosphates*”, Electrochimica Acta, **52** (2007) 4024 – 4031
68. H. Shi, E.-H. Han, F. Liu, “*Corrosion protection of aluminium alloy 2024-T3 in 0.05 M NaCl by cerium cinnamate*”, Corrosion Science, **53** (2011) 2374 – 2384

69. S. Kozhukharov “*Relationship between the conditions of preparation by the sol-gel route and the properties of the obtained products*” Journal of the University of Chemical Technology and Metallurgy, **44**, 2, (2009) 143 – 150
70. Kozhukharov, S. Tchaoushev „*Perspectives for development and industrial application of spray pyrolysis method*” ANNUAL PROCEEDINGS OF “Angel Kanchev” University of Ruse, (Bulgaria); Volume **50**, issue 9.1 (2011), pp. 46 – 50, accessible via: http://fr.uni-ruse.bg/download/konferencia/konf_2011_9_1.pdf
71. Kozhukharov S, G.. Tsaneva, V. Kozhukharov, J. Gerwann, M. Schem, T. Schmidt, M. Veith “*Corrosion protection properties of composite hybrid coatings with involved nanoparticles of zirconia and ceria*” Journal of the University of Chemical Technology and Metallurgy, **43**, 1, (2008) 73 – 80
72. B.R.W. Hinton, J. Alloys Compounds **180** (1992) 15.
73. W. G. Fahrenholtz, M. J. O’Keefe, H. Zhou, J.T. Grant “*Characterization of cerium-based conversion coatings for corrosion protection of aluminum alloys*” Surface and Coatings Technology **155** (2002) 208 – 213
74. Berny F. Rivera, Benedict Y. Johnson, Matthew J. O’Keefe, William G. Fahrenholtz “*Deposition and characterization of cerium oxide conversion coatings on aluminum alloy 7075-T6*” Surface and Coatings Technology **176** (2004) 349 – 356
75. D. Zhao, J. Sun, L. Zhang, Y. Tan, J. Li, “*Corrosion behavior of rare earth cerium based conversion coating on aluminum alloy*” Journal of Rare Earths, **28**, (2010), p. 371 – 374
76. I. Aziz, Z. Qi, X. Min “*Corrosion Inhibition of SiCp/5A06 Aluminum Metal Matrix Composite by Cerium Conversion Treatment*” Chinese Journal of Aeronautics **22**, (2009) 670 – 676
77. B. Pentchev, S. Detchev, *Manual of Galvano-techniques* ,Technika, Sofia 1982 (in Bulgarian).
78. L.Y. Kadaner, *Manual of Galvanostegy*, Technika Gov. Ed., Kiev, 1976 (in Russian)
79. I. Gadzhov “*Manual for Galvanotechniques*” Sofia (2008), p. 87
80. M. J. O’Keefe, S. Geng, S. Joshi, “*Cerium-Based Conversion Coatings as Alternatives to Hex Chrome*” metalfinishing, (2007), 25 – 28

81. B. F. Rivera, B. Y. Johnson, M. J. O'Keefe, W. G. Fahrenholtz "Deposition and characterization of cerium oxide conversion coatings on aluminum alloy 7075-T6" *Surface and Coatings Technology* **176** (2004) 349 – 356
82. W. Pinc, S. Geng, M. O'Keefe, W. Fahrenholtz, T. O'Keefe, "Effects of acid and alkaline based surface preparations on spray deposited cerium based conversion coatings on Al 2024-T3" *Applied Surface Science* **255** (2009) 4061 – 4065
83. S. Geng, S. Joshi, W. Pinc, W.G. Fahrenholtz,⁽¹⁾M.J. O'Keefe, T.J. O'Keefe, and P. Yu "Influence of processing parameters on cerium based conversion coatings" Proceed "TRI – Service – 2007" - corrosion conference: Accessible via: <https://www.corrdefense.org/Technical%20Papers/Influence%20of%20Processing%20Parameters%20on%20Cerium%20Based%20Conversion%20Coatings.pdf>
84. K. A. Yasakau, M. L. Zheludkevich, S. V. Lamaka and M. G. S, Ferreira: *Mechanism of Corrosion Inhibition of AA2024 by Rare-Earth Compounds*, *Journal of Physical Chemistry B*, **110** (2006) pp. 5515 – 5528
85. A. Conde, M.A. Arenas, A. de Frutos, J. de Damborenea "Effective corrosion protection of 8090 alloy by cerium conversion coatings" *Electrochimica Acta* **53** (2008) 7760 – 7768
86. D. K. Heller, W. G. Fahrenholtz, M. J. O'Keefe "The effect of post-treatment time and temperature on cerium-based conversion coatings on Al 2024-T3" *Corrosion Science* **52** (2010) 360 – 368.
87. M. Bethencourt, F.J. Botana, M.J. Cano, M. Marcos, J.M. Sánchez-Amaya, L. González-Rovira, *Behaviour of the alloy AA2017 in aqueous solutions of NaCl. Part I: Corrosion mechanisms*, *Corrosion Science*, **51** (2009) 518 - 524.
88. R.G. Buchheit, R.P. Grant, P.F. Hlava, B. McKenzie, G.L. Zender, *Local Dissolution Phenomena Associated with S Phase (Al₂CuMg) Particles in Aluminum Alloy 2024-T3*, *Journal of the Electrochemical Society*, **144** (1997) 2621 - 2628.
89. A. Boag, A.E. Hughes, A.M. Glenn, T.H. Muster, D. McCulloch, *Corrosion of AA2024-T3 Part I: Localised corrosion of isolated IM particles*, *Corrosion Science*, **53** (2011) 17 -26.

90. E. Hughes, A. Boag, A.M. Glenn, D. McCulloch, T.H. Muster, C. Ryan, C. Luo, X. Zhou, G.E. Thompson “*Corrosion of AA2024-T3 Part II: Co-operative corrosion*” Corrosion Science, **53** (2011) 27 - 39.
91. R. H. Petrucci, W. S. Harwood, “*General Chemistry. Principles and modern applications*” Prentice Hall Iberia S. R. L. (Madrid) –(1999); 730; ISBN: 84-8322-043-1.
92. http://en.wikipedia.org/wiki/Optical_microscope
93. M. C. D’Ocon, M. J. Garcia, J. C. Vicente, “*Fundamentos y tecnicas de analisis bioquimico. Principios de analisis instrumental*” Editorial Paraninfo, ITP An International Thomson Publishing company (Madrid) – (1999); **150**; ISBN: 84-283-2501-4.
94. http://www.splav.kharkov.com/en/e_mat_start.php?name_id=1438
95. S. Kozhukharov, V. Kozhukharov, M. Wittmar, M. Schem, M. Aslan, M. H. Caparotti, M. Veith “*Protective abilities of nanocomposite coatings containing Al₂O₃ nano-particles loaded by CeCl₃*” Progress in Organic Coatings **71** (2011) 198 – 205
96. A. A. Salve, S. Kozhukharov, J. E. Pernas, E. Matter, M. Machkova, “A Comparative research on hybrid nano-composite protective primary coatings for AA2024 aircraft alloy” Journal of the University of Chemical Technology and Metallurgy **47** (3), (2012) 319 – 326
97. M. Bethencourt, F.J. Botana, M.J. Cano, M. Marcos, J.M. Sánchez-Amaya, L. González-Rovira, Corros. Sci. **51** (2009) 518-524.

98. J.E. Pernas, S. Kozhukharov, A.A Salves, E. Matter, M. Machkova, “Influence of the oxidation state of Ce-ions on the inhibition of AA2024 Alloy corrosion in a model corrosive ” *Journal of the University of Chemical Technology and Metallurgy* **47** (3), (2012) 311 – 318